

Effect of methanol on the phase-transition properties of glycerol-monopalmitate lipid bilayers investigated using molecular dynamics simulations: In quest of the biphasic effect

Monika Laner, Philippe H. Hünenberger*

Laboratory of Physical Chemistry, ETH Zürich, Zürich, Switzerland



ARTICLE INFO

Article history:

Available online 7 November 2014

Keywords:

Molecular dynamics
Lipid bilayer
Monoglyceride
Phase transition
Methanol
Biphasic effect

ABSTRACT

The effect of methanol on the phase and phase-transition properties of a $2 \times 8 \times 8$ glycerol-1-monopalmitate bilayer patch is investigated using a series of 239 molecular dynamics simulations on the 180 ns timescale, considering methanol concentrations c_M and temperatures T in the ranges 0–12.3 M and 302–338 K, respectively. The results in the form of hysteresis-corrected transition temperatures T_m are compatible with the expected features of the biphasic effect, with a reversal concentration c_{rev} of about 5.2 M. Below this concentration, the main transition is between the liquid crystal (LC) and gel (GL) phases, and T_m decreases upon increasing c_M . Above this concentration, the interdigitated (ID) phase is the stable ordered phase instead, and T_m slightly increases upon increasing T up to about 10 M. The analysis of the structural and dynamical properties also reveals very different sensitivities and responses of the three phases to changes in c_M . In particular, the properties of the GL phase are insensitive to c_M , whereas those of the LC and ID phases are altered via an increase of the area per lipid. For the LC phase, increasing c_M promotes disorder and fluidity. For the ID phase, in contrast, increasing c_M up to about 10 M slightly increases the ordering and rigidity. Two side issues are also addressed, concerning: (i) the occurrence tilt-precession motions in the GL and ID phases; (ii) the influence of the pressure coupling scheme employed in the simulations, semi- or fully-anisotropic, on the simulation results.

© 2014 Elsevier Inc. All rights reserved.

1. Introduction

Lipid bilayers, the main component of biological membranes, are of crucial importance for all living organisms because they form a barrier separating different cellular compartments, define the boundary of the cell, and represent its first interaction site with the extracellular medium [1]. Aqueous lipids can present many different phases [2,3] depending on the types of the lipid molecules, the extent of hydration and the composition of the aqueous phase, as well as on pressure and temperature. The two biologically most relevant of these phases are bilayer phases, namely the gel (GL) and the liquid crystal (LC) phases (Fig. 1, two bottom left panels). They can be distinguished by the arrangement of the lipids within the bilayer as well as by differences in the area per lipid, in the bilayer thickness and in other properties. In the GL phase, the aliphatic lipid

tails are arranged in nearly all-*trans* conformations and in orientations that are generally tilted with respect to the bilayer normal [2]. In the LC phase, the aliphatic tails are conformationally disordered (mixture of *trans* and *gauche* conformations) and no preferential collective orientation of the chains (tilting) is observed. For a given bilayer composition and given specified environmental conditions, the temperature at which the GL \leftrightarrow LC transition occurs is called the main transition (or melting) temperature T_m . Characterizing the transition temperature of lipid bilayers and the influence of composition and environment on this temperature is of fundamental biological and technological importance [2,4].

There are three basic mechanisms by which the mechanical and permeability properties of the cell membrane can be modulated by cosolutes present in the intra- or extra-cellular medium: (i) direct interaction of the cosolute molecules with specific membrane-bound proteins such as ion or water channels [5–8]; (ii) direct alteration of the phase properties (structure, fluidity, melting temperature) of the bilayer induced by lipid-cosolute interactions [9–12]; (iii) indirect modulation of the properties of membrane-bound proteins via an alteration of the bilayer phase properties [13–16]. While the first type of mechanism implies the existence

* Corresponding author at: Laboratory of Physical Chemistry, ETH Hönggerberg, HCI, CH-8093 Zürich, Switzerland. Tel.: +41 44 632 55 03; fax: +41 44 632 10 39.

E-mail addresses: monika.laner@igc.phys.chem.ethz.ch (M. Laner), phil@igc.phys.chem.ethz.ch (P.H. Hünenberger).

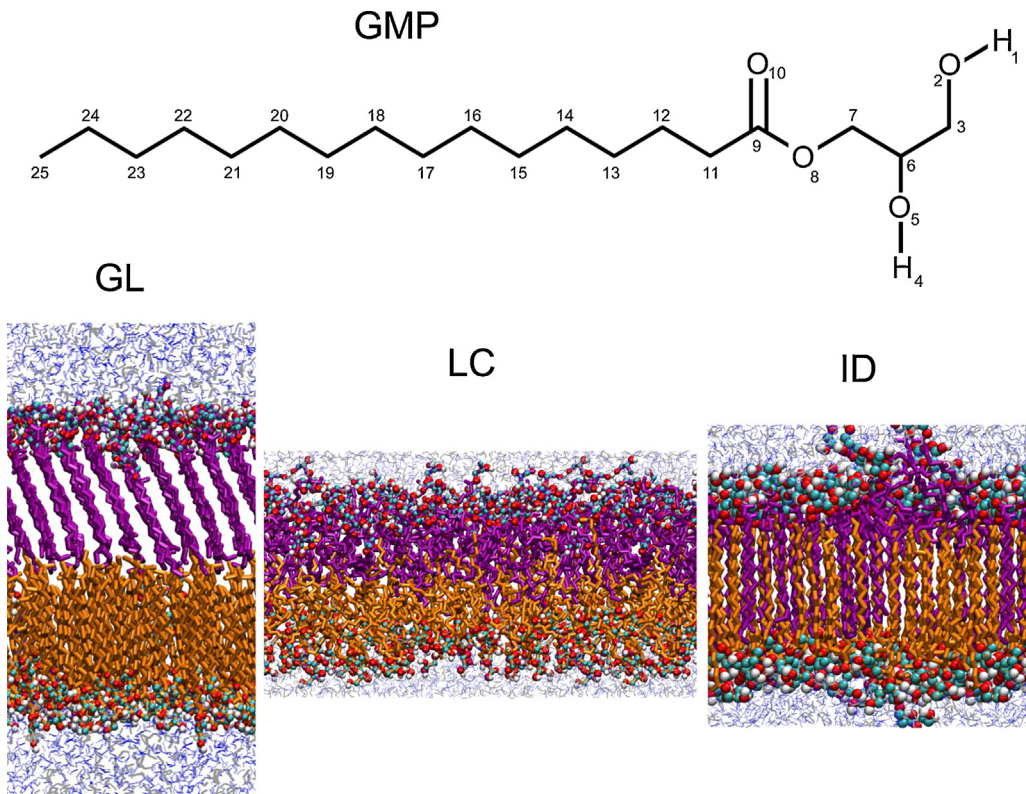


Fig. 1. Chemical structure and bilayer phases of the monoglyceride considered in the present study. The top panel shows the lipid considered, glycerol-1-monopalmitate (GMP), the numbering referring to the GROMOS molecular topology used in the simulations. See Ref. [81] and Suppl. Mat. therein for detailed force-field information. The three bottom panels show illustrative structures for the three phases, gel (GL), liquid crystal (LC) and interdigitated (ID), occurring in the simulations (trajectory frames at 60, 240 and 600 ns, respectively in simulation M_EF_{GL}310 of Ref. [81]). The lipids are colored in orange and purple to distinguish the two leaflets (bottom and top, respectively). MET molecules are displayed in grey and water molecules in blue. The atoms of the headgroup are colored according to the element (C1, C2, C3: light blue, O1, O2, O3: red, and H1, H2: white). Note that the structure for LC is shown along the x-axis of the box, while the structures for GL and ID were rotated around the z-axis to highlight the structural characteristics (alignment or interdigitation). The simulation labels and conditions are summarized in Table 1. (For interpretation of the references to color in this figure legend, the reader is referred to the web version of the article.)

of a specific protein receptor for the cosolute, the two others rely on a generic form of lipid–cosolute interactions. Important mechanisms of the second and third types are responsible, respectively, for the phenomena of anhydrobiosis in the presence of, e.g. sugars [9,17–20] and of anesthesia in the presence of, e.g. xenon [12], alcohols [11,21] or other small molecules [21].

The phenomenon of anesthesia [15,16,22] corresponds to a reversible loss of consciousness caused by an anesthetic drug. Other attributes such as immobility, analgesia, amnesia and muscle relaxation are closely connected to this phenomenon [15,23]. The exact mechanism of anesthesia is still matter of debate [15,21,24,25]. Depending on the type of anesthetic, it may involve either an interaction with specific receptors [15,16,22,23,26], a direct alteration of the membrane properties [22,25,27], or an indirect influence on membrane-bound proteins [28]. In the apparent absence of specific protein receptors for aliphatic alcohol molecules [3,16], it seems that the mechanism of anesthesia relies in this case on an indirect modulation of the properties of membrane-bound proteins via an alteration of the bilayer phase properties [25].

The interaction of alcohols with membranes is further complicated by the biphasic effect [29]. Depending on the concentration range, short-chained aliphatic alcohols have an opposite influence on T_m . At low concentrations, T_m decreases with increasing alcohol concentration, whereas at high concentrations, the opposite trend is observed. The biphasic reversal concentration c_{rev} at which this inversion takes place strongly depends on the nature of the alcohol [30] and on the length of the lipid acyl chains [29]. The biphasic effect is explained by the alcohol-induced formation of an interdigitated (ID) phase (Fig. 1, bottom right panel), where

lipid molecules from the two leaflets of the bilayer interpenetrate [31–34]. At low alcohol concentrations, the GL phase is increasingly destabilized relative to the LC phase, due to the intercalation of alcohol molecules between the lipid headgroups and the resulting increase in the area per lipid, leading to the observed T_m decrease. At high concentrations, the ID phase can be formed, its stability relative to the LC phase increasing with the alcohol concentration, leading to the observed T_m increase. Note that this description relies on a slightly “informal” definition of T_m , which characterizes in the usual way a GL \leftrightarrow LC transition below c_{rev} , but an alternative ID \leftrightarrow LC transition above c_{rev} .

The occurrence of an ID phase at high alcohol concentrations can be interpreted as an extreme consequence of the same effect that induces the T_m decrease at lower concentrations, namely the intercalation of the alcohol molecules between the lipid headgroups [32–36]. This results in an increase of the effective headgroup volume, inducing a lateral expansion in the interfacial region [37–39]. When this expansion is sufficiently pronounced, the void spaces within the bilayer interior can be removed through interdigitation of the lipid tails [31–34,36–41]. All short-chain aliphatic alcohols, from methanol (MET) through heptanol, induce interdigitation at sufficiently high concentrations [30,37,40,41]. However, longer chain alcohols may lead to a different response, presumably because their aliphatic chains are also able to intercalate between the lipid tails [42–44].

Atomistic molecular dynamics (MD) simulations have greatly contributed to the characterization and understanding of the structure, thermodynamics and dynamics of lipid bilayers under various conditions [10,45,21,51,46–50,11,52–62]. These

simulations provide information at a spatial (atomic level) and temporal (femtosecond) resolution inaccessible to experiment, concerning system sizes (~ 10 nm) and timescales ($\sim 1 \mu\text{s}$) already relevant for the evaluation of thermodynamic properties via statistical mechanics and the comparison with experimental data.

The interaction of alcohols with lipid membranes has already been the scope of numerous MD studies, at the atomistic [10,11,48,53,63,64] but also coarse-grained [44,63] levels of resolution. Most of these studies focused on phospholipids such as dipalmitoylphosphatidylcholine (DPPC) and short-chain aliphatic alcohols such as MET or ethanol. However, the biologically most relevant phospholipids including DPPC remain relatively challenging to simulate, owing to difficulties in the force-field design [65,66] and treatment of electrostatic interactions [65,67–73] (charged or zwitterionic headgroup), and to the slow convergence of system properties with respect to both system size [57,66,74–78] (long-range correlations) and simulation timescale [74,75,78–80] (slow conformational relaxation). For this reasons, it is also interesting to consider less complex bilayer systems such as monoglyceride lipid systems [54,56,57,60,61,81].

A (saturated) monoglyceride is the molecule resulting from the esterification of a single hydroxyl group of glycerol with a (saturated) fatty acid. In addition to being relevant in the context of prebiotic research [82,83] and technological applications [84,85], these lipids present a number of key advantages compared to, e.g. DPPC for a computational investigation of lipid phase-transition properties and their modulation by alcohol cosolutes: (i) the presence of only one aliphatic tail per headgroup, leading to a faster translational, rotational, and conformational relaxation; (ii) the limited role of electrostatic interactions (uncharged, non-zwitterionic and moderately polar headgroup), also leading to a faster relaxation and largely avoiding finite-size and approximate-electrostatics artifacts; (iii) the absence of a ripple phase [86] as an intermediate state between the GL and the LC phases; (iv) the availability of experimental structural and thermodynamic data [85,84,87–94]. Here, glycerol-1-monopalmitate (GMP; Fig. 1, top panel) was chosen as model lipid in view of the availability of a phase diagram for the GMP-water system [54,84] and of experimental estimates for the area per lipid in the GL and LC phases [88].

In a previous simulation study by our group [81] (see also Ref. [60]), it was shown that MET has little effect on the GL phase of GMP bilayers, but induces a concentration-dependent lateral expansion in the LC phase, leading to an increase in fluidity and disorder. It was also observed that the heating of a GL structure resulted in a GL \rightarrow LC transition above a certain temperature, this threshold temperature decreasing with increasing MET concentration (318, 314 and 310 K for c_M of 6.0, 9.5 and 12.3 M, respectively). In contrast, the quenching of a LC structure at low temperatures (302 or 306 K) resulted in a LC \rightarrow ID transition instead. In addition, one simulation with $c_M = 12.3$ M initiated from the GL phase and carried out at 310 K evidenced successive GL \rightarrow LC and LC \rightarrow ID transitions. These results are in line with the hypothesis that alcohols promote anesthesia by directly influencing the lipid bilayer properties, thereby indirectly influencing membrane-bound proteins. However, considering that the c_M concentrations considered in the simulations are likely above c_{rev} , they raise a number of questions concerning the relative (meta)stabilities of the GL and ID phases, the kinetic reversibilities of the different transitions on the simulated timescale, the impact of hysteresis on the simulation results, and the correct interpretation of the simulation results in terms of the biphasic effect.

To shed more light on these issues, the present study investigates more systematically the effect of varying the MET concentration on the phase and phase-transition properties of a $2 \times 8 \times 8$ GMP bilayer patch. It also addresses two side issues: (i)

the possible occurrence of collective tilting in the ID phase, and the nature of the associated tilt-precession motions [60]; (ii) the influence of the pressure coupling scheme employed in the simulations, semi- or fully-anisotropic, on the simulation results.

2. Methods

2.1. Molecular dynamics simulations

All MD simulations were performed using the GROMOS MD++ program [95–97], with the 53A6OXY force field [98] for GMP and MET, along with the simple point charges (SPC) water model [99]. More detailed force-field information concerning these simulations can be found in Ref. [81] and Suppl. Mat. therein.

The simulations were carried out under periodic boundary conditions based on rectangular boxes containing a hydrated GMP bilayer patch of $2 \times 8 \times 8$ lipid molecules (two opposite leaflets in the xy-plane, each containing 8×8 molecules), leading to a total number of 128 lipid molecules in the systems. Both leaflets consisted of a racemic mixture of the R and S enantiomers of GMP. The simulations were performed at full hydration with systems containing $N_W = 853$ water molecules. The full hydration regime was defined based on the phase diagram of the GMP water system [54,84], where the main transition temperature T_m is seen to become independent of the hydration level above 36% (w/w) water content (about 6.7 water molecules per lipid). A variable number n_M of MET molecules was also added (see Section 2.2).

Newton's equations of motion were integrated using the leap-frog scheme [100] with a timestep of 2 fs. All GMP and MET bond lengths were constrained by application of the SHAKE procedure [101] with a relative geometric tolerance of 10^{-4} . The full rigidity of the water molecules was enforced by application of the SETTLE procedure [102]. The center of mass translational motion of the computational box was removed every 0.2 ps.

The simulations were carried out in the NPT ensemble with a reference pressure P of 1 bar and reference temperatures T ranging from a minimal temperature T_{\min} (302, 306 or 318 K, depending on the system) to 338 K in steps of 4 K. The temperature was maintained by weakly coupling [103] (Berendsen thermostat) the GMP and MET+water degrees of freedom separately to temperature baths at temperature T , using a relaxation time of 0.1 ps. The pressure was maintained by weakly coupling [103] (Berendsen barostat) the particle coordinates and box dimensions in the xy-plane and along the z-axis separately (semi-anisotropic pressure scaling [66]), or along all three axes separately (fully-anisotropic pressure scaling, for selected systems only) to pressure baths at pressure P , using a relaxation time of 1 ps and an isothermal compressibility of 4.575×10^{-4} (kJ mol $^{-1}$ nm $^{-3}$) $^{-1}$ as appropriate for biomolecular systems [104].

The non-bonded interactions were calculated using a twin-range scheme [104,105] with short- and long-range cutoff distances set to 0.8 and 1.4 nm, respectively, and an update-frequency of five timesteps for the short-range pairlist and intermediate-range interactions. A reaction-field correction [106,107] was applied to account for the mean effect of electrostatic interactions beyond the long-range cutoff distance, using a relative dielectric permittivity of 61 as appropriate for the SPC water model [108]. All simulations were carried out for a duration of 180 ns after equilibration, and configurations were saved to file every 10 ps for subsequent analysis.

2.2. Simulated systems

A total number of 239 simulations (180 ns each) were carried out, differing by: (i) the number n_M of MET molecules included in

Table 1

Simulated systems and simulation conditions. For each simulation, the different columns report the simulation label, the number n_M of MET molecules, the MET concentration w_M by weight (relative to the lipids w_M^L or to water w_M^W), the molality b_M (mol MET per kg water) and the molarity c_M (mol MET per dm^3 MET-water solution, based on density data from Ref. [109]), the starting configuration (GL for gel or LC for liquid crystal) and the reference temperature T . In all cases, the simulations involve a glycerol-1-monopalmitate (GMP) bilayer patch of $2 \times 8 \times 8$ lipids and $n_W = 853$ water molecules (corresponding to 36% (w/w) water per lipid) and are carried out for 180 ns at the reference pressure $P = 1$ bar. For compactness, a single entry is provided for each set of simulations carried out at different temperatures T (value in Kelvin noted generically T in the simulation label). For example the notation $T \in \{302\text{--}338\}$ indicates a set of six simulations at temperatures T ranging from 302 to 338 K in steps of 4 K, and the notation $T \in \{302, 338\}$ indicates a set of two simulations carried out at temperatures T of 302 and 338 K. All simulations were carried out with semi-anisotropic (SEMI) pressure coupling. A subset of the simulations was also repeated with fully-anisotropic (FULL) pressure coupling. The corresponding labels differ by a f subscript. For example, simulations $N_{120}\text{F}_{\text{GL}}302$ and $N_{120}\text{F}_{\text{GL}}302_f$ involve SEMI and FULL coupling, respectively. The simulation sets that were repeated are marked with a parenthesized f subscript in the table. Note that for simulation sets $N_{480}\text{F}_{\text{GL}}T$ and $N_{480}\text{F}_{\text{LC}}T$, the lowest temperature considered is 302 K as indicated, whereas it is 306 K for sets $N_{480}\text{F}_{\text{GL}}T_f$ and $N_{480}\text{F}_{\text{LC}}T_f$.

Simulation	n_M	w_M^L (w/w%)	w_M^W (w/w%)	b_M (mol kg^{-1})	c_M (mol dm^{-3})	Starting configuration	T
$N_0\text{F}_{\text{GL}}T$	0	0.0	0.0	0.0	0.0	GL	$T \in \{318\text{--}338\}$
$N_{120}\text{F}_{\text{GL}}T_f$	120	9.1	25.0	7.8	6.0	GL	$T \in \{302\text{--}338\}$
$N_{240}\text{F}_{\text{GL}}T_f$	240	18.2	50.0	15.6	9.5	GL	$T \in \{302\text{--}338\}$
$N_{360}\text{F}_{\text{GL}}T$	360	27.3	75.0	23.4	11.4	GL	$T \in \{302\text{--}338\}$
$N_{400}\text{F}_{\text{GL}}T$	400	30.3	83.4	26.0	11.8	GL	$T \in \{302\text{--}338\}$
$N_{440}\text{F}_{\text{GL}}T$	440	33.3	91.7	28.6	12.1	GL	$T \in \{302\text{--}338\}$
$N_{480}\text{F}_{\text{GL}}T_f$	480	36.4	100.0	31.2	12.3	GL	$T \in \{302\text{--}338\}$
$N_0\text{F}_{\text{LC}}T$	0	0.0	0.0	0.0	0.0	LC	$T \in \{318, 338\}$
$N_{40}\text{F}_{\text{LC}}T$	40	3.0	8.3	2.6	2.4	LC	$T \in \{302\text{--}338\}$
$N_{80}\text{F}_{\text{LC}}T$	80	6.1	16.7	5.2	4.3	LC	$T \in \{302\text{--}338\}$
$N_{120}\text{F}_{\text{LC}}T_f$	120	9.1	25.0	7.8	6.0	LC	$T \in \{302\text{--}338\}$
$N_{160}\text{F}_{\text{LC}}T$	160	12.1	33.4	10.4	7.4	LC	$T \in \{302\text{--}338\}$
$N_{200}\text{F}_{\text{LC}}T$	200	15.1	41.7	13.0	8.5	LC	$T \in \{302\text{--}338\}$
$N_{240}\text{F}_{\text{LC}}T_f$	240	18.2	50.0	15.6	9.5	LC	$T \in \{302\text{--}338\}$
$N_{280}\text{F}_{\text{LC}}T$	280	21.2	58.4	18.2	10.3	LC	$T \in \{302\text{--}338\}$
$N_{320}\text{F}_{\text{LC}}T$	320	24.2	66.7	20.8	10.9	LC	$T \in \{302\text{--}338\}$
$N_{360}\text{F}_{\text{LC}}T$	360	27.3	75.5	23.4	11.4	LC	$T \in \{302\text{--}338\}$
$N_{400}\text{F}_{\text{LC}}T$	400	30.3	83.4	26.0	11.8	LC	$T \in \{302\text{--}338\}$
$N_{440}\text{F}_{\text{LC}}T$	440	33.3	91.7	28.6	12.1	LC	$T \in \{302\text{--}338\}$
$N_{480}\text{F}_{\text{LC}}T_f$	480	36.4	100.0	31.2	12.3	LC	$T \in \{302\text{--}338\}$

the simulated system (from 0 to 480 in steps of 40); (ii) the initial configuration (GL vs. LC); (iii) the temperature T (from $T_{\min} = 302$, 306 or 318 K, depending on the system, to 338 K in steps of 4 K); (iv) the pressure-coupling scheme (SEMI for semi-anisotropic vs. FULL for fully-anisotropic). Only a subset of the possible combinations was considered. For the simulations initiated from the GL phase, only simulations with $n_M = 0, 120, 240, 360, 400, 440$ and 480 MET molecules were performed. The minimal temperature T_{\min} considered was generally set to 302 K, with two exceptions. For the systems without MET, a value of 318 K was used instead, and for the system with $n_M = 480$ and FULL pressure coupling, a value of 306 K was used instead. The simulation temperature was systematically varied from T_{\min} to 338 K in steps of 4 K with two exceptions. For the simulations initiated from the LC phase, either without MET or with $n_M = 480$ and FULL pressure coupling, only the extreme temperatures of T_{\min} and 338 K were considered. Finally, although all the combinations were considered with SEMI pressure coupling, only a subset was repeated with FULL pressure coupling. A summary of the simulated systems and simulation conditions is provided in Table 1.

In this article, each simulation is uniquely identified by a string consisting in sequence of the letters N (generic for GMP-MET-water systems), the number of MET molecules (subscript), the letter F (full hydration), the letters GL or LC (starting structure; subscript), the temperature T , and the optional letter f (FULL pressure coupling; subscript). For example, the simulation including 120 MET molecules initiated from a GL structure and carried out at 302 K using SEMI pressure coupling is labeled $N_{120}\text{F}_{\text{GL}}302$, the corresponding simulation using FULL pressure coupling being labeled $N_{120}\text{F}_{\text{GL}}302_f$.

The simulations without MET ($n_M = 0$) were reported previously in Ref. [57] (system B_L therein) and in Ref. [81] (system P_N therein). The simulations with $n_M = 120, 240$, or 480 and FULL pressure coupling were reported previously in Ref. [81] (systems M_L , M_M , and M_F , respectively, therein). Note that the simulations were analyzed over a 600 ns time period in Refs. [57,81], whereas only the first 180 ns of these simulations are considered here, for consistency

with the additional simulations. The initial configurations for the systems N_0, N_{120}, N_{240} and N_{480} were generated as described in Ref. [81]. The initial configurations for the other systems were generated following the same procedure with the appropriate value of n_M . All production simulations were initiated directly from these initial configurations and carried out at the indicated simulation temperatures (no additional thermalization step).

For the ease of comparison with experimental data, the MET concentrations, as determined by the MET content n_M and the number $n_W = 853$ of water molecules, are reported for the different systems in Table 1. In principle, molal concentrations b_M (mol MET per kg water) should be preferred owing to their independence of the mixture density. However, since experimental studies typically rely on molarities c_M instead (unit symbol M, i.e. mol MET per dm^3 MET–water solution), the corresponding values are also reported (based on density data from Ref. [109]) and will be used for the discussion.

2.3. Trajectory analysis

The simulations were analyzed in terms of the following properties: (i) phase-assignment descriptor η ; (ii) area per lipid a_{xy} ; (iii) bilayer thickness d_z ; (iv) volume per lipid v_{xyd} ; (v) carbon–hydrogen order parameters $S_{\text{CH}}(C_n)$ of the 14 methylene groups (C_n , with $n = 2\text{--}15$) and corresponding chain-averaged value S_{chn} ; (vi) hydrogen-bonding (H-bonding) properties; (vii) single-lipid and collective apical tilt angles θ and Θ , respectively, describing the orientation of the aliphatic tails relative to the bilayer normal; (viii) single-lipid and collective azimuthal tilt angles ϕ and Φ , respectively, describing the orientation of the aliphatic tails projected onto the bilayer plane; (ix) lipid lateral diffusion coefficients D_{xy} ; (x) lipid rotational (R) or wobbling (W) relaxation times τ and residual correlations $c(\tau_1^R, c_1^R, \tau_2^R, c_2^R, \tau_1^W, c_1^W, \tau_2^W, c_2^W)$; distinguishing fast and slow decays by the indexes 1 and 2.

The procedures employed for these analyses have been described previously [54,57,60,81] and this information will not be repeated here. For the phase-assignment descriptor, the

following parameters were used for all systems, which differ slightly from those of Ref. [81] (see Eq. (1) therein): $a_c = 0.305 \text{ nm}^2$, $a'_c = 0.29 \text{ nm}^2$, $h_c = 3.9 \text{ nm}$, $h'_c = 3.8 \text{ nm}$ and $t_c = -0.3 \text{ nm}$.

3. Results and discussion

3.1. Phase transitions

To characterize the influence of the MET concentration on the phase-transition temperature T_m of the bilayer, the 188 simulations carried out with SEMI pressure coupling are considered here. The possible occurrence of phase transitions along these simulations was detected by monitoring the time series of the phase-assignment descriptor η (Eq. (1) in Ref. [81] with parameters given in Section 2.3). This indicator relies on three structural characteristics (area per lipid, distance between the planes of the headgroup glycerol central carbon atoms, bottom-to-top distance between the planes of the tail methyl groups) to ascribe each trajectory configuration to a given phase (LC, GL or ID), or leave it unassigned (UN) if the values do not fall within appropriate ranges for either of these three phases. The corresponding time series are displayed graphically in Fig. 2 for the 188 simulations.

Three types of transitions are observed, depending on the initial phase, the MET concentration and the simulation temperature: (i) GL → LC transitions for simulations initiated from the GL phase and carried out at high temperatures; (ii) LC → GL transitions for simulations initiated from the LC phase and carried out at low MET concentrations ($n_M = 40, 80$) and low temperatures; (iii) LC → ID transitions for simulations initiated from the LC phase and carried out at higher MET concentrations ($n_M \geq 120$) and low temperatures.

For the simulations undergoing a transition, the time to transition is generally correlated with the temperature. For example, for the GL → LC transitions observed in the range 314–338 K, the time to transition systematically decreases with increasing temperature. The trend is less systematic for the LC → GL and LC → ID transitions observed in the range 302–310 K, where the time to transition only tententially decreases with decreasing temperature. Such approximate correlations are easily understood considering that the driving force associated with a transition, and thus its expected rate assuming a linear response of the kinetics to the thermodynamics, depends on the difference between the system temperature and the equilibrium transition temperature. Their non-systematic nature is also expected considering that the present simulations probe single events in simulations of finite durations, whereas the above correlations formally refer to averages over multiple events, *i.e.* the observation of a correlation based on single-event finite-timescale simulations is likely but not guaranteed [61]. A typical situation of this kind is the observation of a LC → GL transition in the system with $n_M = 80$ and $T = 306 \text{ K}$, apparently incompatible with the absence of such a transition at $T = 302 \text{ K}$. The latter transition would almost certainly occur in an extended simulation.

The occurrence of multiple phase transitions as well as of direct GL → ID transitions was never observed in the simulations. In the former case, however, the situation of two successive transitions has occurred once in Ref. [81] for a system with $n_M = 480$, considering longer simulations of 600 ns with FULL pressure coupling (simulation labeled M_EF_{GL}310 therein, the first 180 ps of which are labeled N₄₈₀F_{GL}310_f in the present article). The latter simulation evidenced a GL → LC transition at 140 ns, followed by a LC → ID transition at 500 ns.

A marginal fraction of unrecognized (UN) configurations typically occurs close to transition points or intermittently at temperatures close to the equilibrium transition temperature. One exception is simulation N₂₀₀F_{LC}306, where ID-like configurations appear after 20 ns, but with a portion of one leaflet remaining in

LC-like disorder, which prevents them from being recognized as ID by the phase-assignment descriptor. An analogous situation has been observed previously in Ref. [81] considering longer simulations of 600 ns with FULL pressure coupling (simulation labeled M_LF_{LC}302 therein, the first 180 ps of which are labeled N₁₂₀F_{LC}302_f in the present article), where ID-like configurations presented some lipids extruded from one leaflet. In the following, these configurations will be considered as belonging to the ID phase.

The observations of Fig. 2 are summarized synoptically in Table 2 in terms of transition occurrences. These results clearly evidence the existence of two regimes depending on the MET content. For $n_M \leq 80$, lowering the temperature of the LC phase leads to a LC → GL transition. For $n_M \geq 120$, this lowering leads to a LC → ID transition instead. In both regimes, however, increasing the temperature of the GL phase leads to a GL → LC transition. The transition concentration c_{rev} , estimated using $n_M = 100$, corresponds to 5.2 M.

A second prominent feature in Table 2 is that the characteristic temperatures for the GL → LC and reverse LC → GL transitions, as well as for the LC → ID and quasi-reverse GL → LC transitions, present a gap of about 5–15 K. The occurrence of such a gap is due to hysteresis effects on the 180 ns simulation timescale. Note that hysteresis may in some cases also be an experimental problem, even for timescales in the range of hours [30]. On a given timescale, a transition will only be observed with a high likelihood if it has a driving force beyond a certain threshold. This in turn implies a minimal temperature difference relative to the equilibrium transition temperature, positive for GL → LC and negative for LC → GL or LC → ID transitions. In another study [61], the influence of the temperature difference to T_m on the time to transition was investigated for the GL ↔ LC transition of GMP based on multiple (10) repeats of 360 ns simulations at each temperature point, and averaging of the corresponding times to transitions. The results of this analysis are summarized in Fig. 3, and suggest that on the 180 ns timescale, a GL → LC transition is likely to be observed for temperatures of at least $T_m + 4 \text{ K}$, and a LC → GL transition for temperatures of at most $T_m - 7 \text{ K}$. As an attempt to correct for these hysteresis effects in an approximate fashion, corresponding offsets of -4 K (GL → LC) and $+7 \text{ K}$ (LC → GL, also assumed valid for LC → ID) can be added to the transition temperature estimates based on Table 2 (midpoint temperatures between simulations evidencing or not a transition). The results are displayed graphically in Fig. 4 (top panel) along with a schematic phase diagram illustrating a possible interpretation of this data (bottom panel).

For MET concentrations c_M below $c_{rev} = 5.2 \text{ M}$, the GL phase is stable at low temperatures and the LC phase at high temperatures. The hysteresis-corrected T_m (between 315 and 320 K in this c_M range) characterizes here the GL ↔ LC transition and decreases with increasing c_M , due to an increase in the effective headgroup cross-section caused by the intercalation of the MET molecules, stabilizing LC over GL. Reversible LC ↔ GL transitions are observed in these simulations upon decreasing the temperature starting from LC phase or increasing the temperature starting from GL phase, albeit with a significant hysteresis (-7 K and $+4 \text{ K}$, respectively) on the 180 ns timescale.

For MET concentrations above c_{rev} , the LC phase is still the stable phase at high temperatures, but the ID phase is now the stable one at low temperatures. The hysteresis-corrected T_m (between 311 and 320 K in this c_M range) characterizes here the ID ↔ LC transition and slightly increases with increasing c_M (up to about 10 M, remaining essentially constant thereafter), due to a further increase in the effective headgroup cross-section caused by the addition of more MET molecules, stabilizing ID over LC. Upon decreasing the temperature starting from the LC phase, LC → ID transitions are observed in the simulations, again with a significant hysteresis (estimated to -7 K). However, the simulations initiated from a GL phase at low temperatures actually sample a metastable phase,



Fig. 2. Time series of the phase-assignment descriptor for a subset of the simulations. Shown is the value of the phase-assignment descriptor η (Eq. (1) in Ref. [81] with parameters given in Section 2.3) for the different simulations starting from a structure appropriate either for the GL phase (top panel) or LC phase (bottom panel) and carried out during 180 ns with semi-anisotropic (SEMI) pressure coupling. They differ in terms of the number n_M of MET molecules and the reference temperature T . The descriptor values are LC (liquid crystal), GL (gel), ID (interdigitated) and UN (unassigned). The simulation labels and conditions are summarized in Table 1.

probably associated with a very long lifetime considering the difficulty of rearranging GL into ID structures without going through LC. Upon increasing the temperature they undergo a GL → LC transition, to a LC phase that may also itself be metastable relative to ID if the temperature is not sufficiently high. The simulation of Ref. [81] undergoing a GL → LC followed by a LC → ID transition on the 600 ns timescale (see above) is consistent with this interpretation, considering that it corresponds to $n_M = 480$ ($c_M = 12.3$ M) and $T = 310$ K, precisely in the region where the LC phase is expected to be metastable relative to ID. Note that the cross-over point between the hysteresis-corrected T_m for LC ↔ GL and LC ↔ ID is at about $n_M = 180$ ($c_M = 8.0$ M), which is slightly above $c_{rev} = 5.2$ M and

represents an alternative estimate for this reversal concentration based on the simulations

To our knowledge, there is no experimental estimate for the biphasic reversal concentration of GMP in the presence of MET. However, the present simulation estimate for this threshold, $c_{rev} = 5.2$ M, can be qualitatively compared to corresponding experimental values of 1.40 M [110] for distearoylphosphatidylcholine (DSPC) and MET, 2.5 M [30,36] or 2.7 M [111] for DPPC and MET, or 1.09 M ([43]; upper bound) for DPPC and ethanol. Clearly, however, quantitative agreement should not be expected considering that c_{rev} can vary widely depending on the nature of the alcohol, on the number and lengths of the lipid tails, and on the type of

Table 2
Occurrence of a phase transition for a subset of the simulations. The simulations were started from a structure appropriate for the GL phase or the LC phase and carried out during 180 ns with semi-anisotropic (SEMI) pressure coupling. They differ in terms of the number n_M of MET molecules and the reference temperature T . A minus (–) indicates the absence of a transition, a cross (×) the presence of a GL → LC transition, a triangle (Δ) the presence or a LC → GL transition and a circle (○) the presence of a LC → ID transition. The simulation labels and conditions are summarized in Table 1.

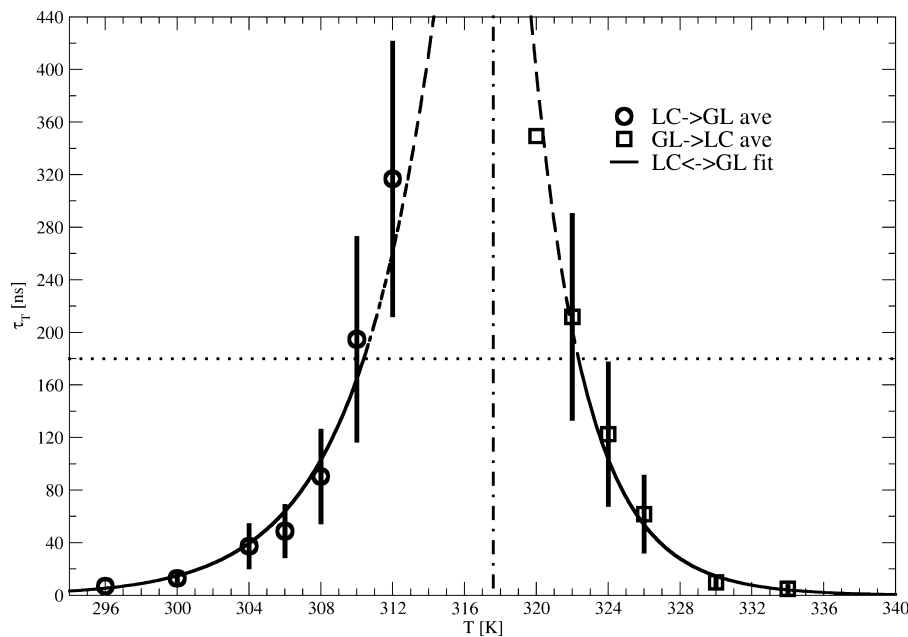


Fig. 3. Average time to transition as a function of the simulation temperature T . The average time to transition τ_T averaged over 10 independent simulations started from a structure appropriate for the LC phase and carried out at reference temperatures in the range 296–312 K (circles), or from a structure appropriate for the GL phase and carried out at reference temperatures in the range 320–334 K (squares), are reported as a function of the temperature T . The bars indicate the error on the mean. Fitting curves for the forward and backward $GL \leftrightarrow LC$ transition times are also displayed. The two curves cross at the transition temperature $T_m = 317.6$ K as indicated by a vertical line. The 180 ns timescale of the present simulations is also indicated with a horizontal line. The data is taken from Ref. [61] (note that the average residence time is displayed therein, i.e. $2\tau_T$ instead of τ_T).

headgroup functionalization. On the other hand, the hysteresis-corrected estimate of T_m in the absence of MET at full hydration ($c_M = 0$ point in Fig. 4), about 320 K, compares well with the experimental value[54,84] of 323 K.

The interpretation of Fig. 4 (top and bottom) given above is plausible and compatible with the expected features of the biphasic effect. However, this interpretation remains to be further validated by means of: (i) longer simulations to reduce the hysteresis ranges; (ii) simulation repeats to increase the statistical accuracy; (iii) additional simulations with $c_M \geq c_{rev}$ initiated from the stable ID phase rather than from the metastable GL phase.

3.2. Phase properties

To characterize the influence of the MET concentration on the structural and dynamic properties of the bilayer in its three phases, the simulations with SEMI pressure coupling corresponding the lowest (318 K for N_0 and 302 K for all other systems) and the highest (338 K) temperatures considered at each methanol content are discussed here. In this subset of 40 simulations, the starting phase is either thermodynamically stable (no transition) or very unstable (early transition), so that an analysis of these trajectories over their last 24 ns characterizes a single and well-equilibrated final phase. The average values of key structural properties calculated over this time period for the different simulations are reported in Table 3 and illustrated graphically in Figs. 5 and 6. Other properties are displayed graphically in Figs. 7 and 8 (H-bonding properties) as well as Fig. 9 (dynamic properties), the corresponding numerical values being listed in Suppl. Mat. Tables S.1, S.2 and S.3, respectively. Finally, the corresponding averages for the entire set of 188 simulations with SEMI pressure coupling can be found in Suppl. Mat. Tables S.4, S.5 and S.6, and S.7, respectively.

The quantities displayed in Fig. 5 (data in Table 3) as a function of the temperature T for the different MET concentrations c_M are the area per lipid a_{xy} , the chain-averaged order parameter S_{chn} and the bilayer thickness d_z . The upper part of the figure

corresponds to simulations started from the GL phase (a_{xy} , S_{chn} and d_z of about 0.24 nm^2 , 0.32 and 4.0 nm, respectively). Upon increasing T above a threshold depending on c_M , a transition to the LC phase is observed (a_{xy} , S_{chn} and d_z of about 0.32 – 0.44 nm^2 , 0.08–0.16 and 2.4–3.2 nm, respectively). The structural properties of the GL phase are seen to be essentially independent of c_M and T over the range considered. In contrast, those of the LC phase depend strongly on c_M and slightly on T , the trends upon increasing either c_M or T being the same, namely an increase in a_{xy} and a decrease in S_{chn} and d_z . The lower part of the figure corresponds to simulations started from the LC phase. Upon decreasing T below a threshold depending on c_M , a transition to the GL phase is observed if $n_M \leq 80$. Otherwise, the transition is to the ID phase (a_{xy} , S_{chn} and d_z of about 0.32 – 0.37 nm^2 , 0.35–0.42 and 2.2–2.7 nm, respectively). The same trends are observed as above concerning the sensitivity of the properties of the LC phase with respect to c_M and T . Corresponding trends for the GL and ID phases are difficult to extract from these simulations, because the equilibration of the two phases after a transition from the LC phase is a slow process. As a result, the properties of the final phase after 180 ns still vary significantly depending on the transition history of the system (equilibration time in the final phase). Focusing on the simulations having undergone early transitions, it appears that the properties of the ID phase, just as for the GL phase, are rather insensitive to the temperature over the range considered. However, in contrast to the GL phase, a slight dependence on the MET content can be observed for the ID phase, which is best visible in Fig. 6 (see below).

The quantities displayed in Fig. 6 (data in Table 3) as a function of c_M for the different phases (and at different temperatures for LC) include a_{xy} , S_{chn} and d_z , as well as the volume per lipid v_{xyd} , the single-lipid tilt angle θ (average of the angles between single-lipid head-tail vectors and the bilayer normal), the collective tilt angle Θ (angle between the vector sum of the head-tail vectors of all lipids and the bilayer normal), the distance g between the planes of the tail methyl groups (measured bottom-to-top), and the lateral diffusion coefficient D_{xy} . Here again, the most pronounced and

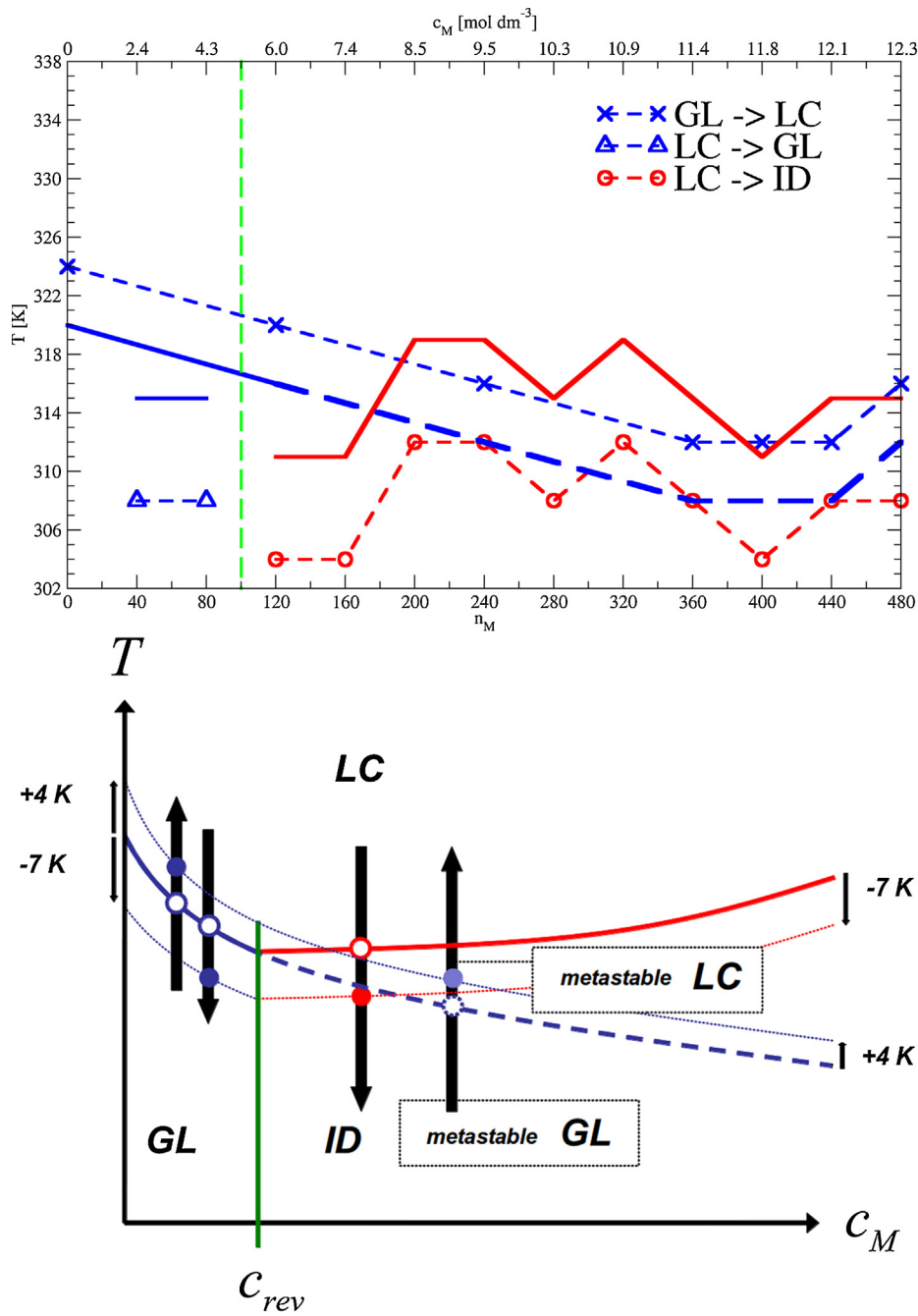


Fig. 4. Transition temperatures, observed in the simulations or hysteresis-corrected, and phase diagram illustrating the interpretation of these results in terms of the biphasic effect. In the top panel, the estimated transition temperatures are shown (dotted lines with symbols), i.e. averages between the lowest T presenting a phase transition and the highest T not presenting a phase transition, as a function of the methanol content n_M or concentration c_M based on the entries of Table 2. Estimated transition temperatures approximately corrected for hysteresis effects by +7 K ($LC \rightarrow GL$ or $LC \rightarrow ID$) and -4 K ($GL \rightarrow LC$) are also displayed (solid lines). The hysteresis-corrected $GL \rightarrow LC$ transitions involving the metastable GL phase are indicated by a long dashed line. The bottom panel provides a tentative interpretation of this data. At high temperature, the LC phase is the most stable. At low temperature, the GL and ID phases are the stable phases below and above c_{rev} , respectively. The arrows indicate the effect of increasing or decreasing the reference temperature in the 180 ns simulations (solid circles) or ideal hysteresis-corrected transition points (open circles). The last arrow on the right, corresponds to probing transitions from a metastable GL phase as done in the present simulations.

systematic dependence of the bilayer properties on the MET concentration is observed for the LC phase, the parameters a_{xy} , θ and D_{xy} presenting a positive correlation, and the parameters S_{chn} , d_z and g a negative correlation with c_M . The parameters v_{xyd} and Θ are essentially constant (see further below). The decrease of the order parameters upon increasing the alcohol concentration has been observed previously in NMR experiments concerning dimyristoylphosphatidylcholine and ethanol [33]. In fact, the primary effect of MET on the LC phase can be viewed as a concentration-dependent

lateral expansion (increase in a_{xy}), due to the intercalation of the MET molecules between the headgroups, as observed in previous experimental [36,39] and simulation studies [10,48,63] of various phospholipids. As discussed in previous articles [60,81], the correlated variation of the other parameters for this phase can be viewed as an indirect consequence resulting from the area increase, namely an increase in the extent of single-lipid tilting (kinking) and of the bilayer fluidity (the latter also visible in the single-lipid rotational and wobbling times; see Fig. 9), and a decrease in the ordering and

Table 3

Average structural properties calculated from a subset of simulations at the highest and lowest temperatures. This subset encompasses the simulations started from a structure appropriate for either the GL phase or the LC phase at reference temperatures of 318 K (system N₀) or 302 K (all other systems) and 338 K, for the different MET concentrations. The quantities reported are the final phase (GL, LC or ID), the area per lipid a_{xy} , the chain-averaged order parameter S_{chn} , the bilayer thickness d_z , the volume per lipid v_{xyd} , the percentage of the configurations assigned to the different phases (GL, LC, or ID, considering the entire 180 ns simulation time), the headgroup–headgroup (glycerol central carbon atom) distance h , the tail–tail (terminal methyl groups, bottom-to-top) distance g , the single-lipid tilt angle θ averaged over all lipids, its root-mean-square deviation in time σ_θ and time-averaged root-mean-square deviation γ_θ across lipids, and the collective tilt angle Θ along with its root-mean-square deviation in time σ_Θ . The quantities (except the percentages spent in the different phases) are averaged over the last 24 ns of the simulation, where all systems are over 90% of the time in the indicated final phase. The simulation labels and conditions are summarized in Table 1. Corresponding data for the entire set of 239 simulations can be found in Tables S.4 and S.10 of the Suppl. Mat. document.

Simulation	Final phase	a_{xy} (nm ²)	S_{chn}	d_z (nm)	v_{xyd} (nm ³)	GL (%)	LC (%)	ID (%)	UN (%)	h (nm)	g (nm)	θ (°)	σ_θ (°)	γ_θ (°)	Θ (°)	σ_Θ (°)
N ₀ F _{GL} 318	GL	0.239	0.307	3.91	0.449	100.0	0.0	0.0	0.0	4.17	0.41	22.0	3.2	9.9	19.5	4.8
N ₀ F _{GL} 338	LC	0.327	0.159	3.17	0.495	0.6	98.7	0.0	0.8	3.32	0.38	32.8	2.9	18.8	7.1	3.6
N ₀ F _{LC} 318	LC	0.301	0.161	3.28	0.485	0.0	61.1	0.0	38.9	3.54	0.37	28.3	2.4	16.9	7.6	3.7
N ₀ F _{LC} 338	LC	0.328	0.155	3.10	0.483	0.0	100.0	0.0	0.0	3.30	0.36	32.7	2.7	18.8	6.8	3.5
N ₄₀ F _{LC} 302	GL	0.245	0.357	4.07	0.476	51.7	6.6	0.0	41.7	4.01	0.17	16.1	2.7	11.3	11.1	3.6
N ₄₀ F _{LC} 338	LC	0.340	0.142	3.01	0.488	0.0	100.0	0.0	0.0	3.23	0.35	33.9	2.3	19.5	6.9	3.5
N ₈₀ F _{LC} 302	LC	0.305	0.188	3.29	0.478	0.0	70.5	0.0	29.5	3.49	0.32	28.4	2.9	17.5	7.6	3.8
N ₈₀ F _{LC} 338	LC	0.354	0.145	2.91	0.490	0.0	100.0	0.0	0.0	3.12	0.32	35.6	3.0	20.2	6.8	3.4
N ₁₂₀ F _{GL} 302	GL	0.235	0.301	3.84	0.429	100.0	0.0	0.0	0.0	4.14	0.33	25.0	1.3	5.4	24.2	1.5
N ₁₂₀ F _{GL} 338	LC	0.366	0.143	2.85	0.495	1.0	98.7	0.0	0.3	3.06	0.28	36.3	3.3	20.3	7.0	3.7
N ₁₂₀ F _{LC} 302	ID	0.324	0.350	2.24	0.345	0.0	43.0	53.5	3.5	3.07	-0.57	20.0	9.1	15.8	9.0	3.5
N ₁₂₀ F _{LC} 338	LC	0.367	0.129	2.91	0.511	0.0	100.0	0.0	0.0	3.04	0.28	36.8	3.1	20.6	7.0	3.6
N ₁₆₀ F _{LC} 302	ID	0.330	0.377	2.49	0.392	0.0	83.1	16.9	0.0	3.08	-0.67	16.1	4.0	19.7	5.9	2.9
N ₁₆₀ F _{LC} 338	LC	0.382	0.138	2.69	0.491	0.0	100.0	0.0	0.0	2.95	0.26	38.1	3.2	21.2	7.2	3.7
N ₂₀₀ F _{LC} 302	ID	0.329	0.367	2.38	0.373	0.0	53.5	46.5	0.0	3.05	-0.59	18.4	10.9	17.3	5.5	2.8
N ₂₀₀ F _{LC} 338	LC	0.394	0.135	2.63	0.491	0.0	100.0	0.0	0.0	2.89	0.21	38.2	3.4	21.4	7.3	3.9
N ₂₄₀ F _{GL} 302	GL	0.234	0.320	4.11	0.459	100.0	0.0	0.0	0.0	4.21	0.37	22.5	2.7	7.7	20.0	4.7
N ₂₄₀ F _{GL} 338	LC	0.405	0.114	2.65	0.514	0.4	99.1	0.0	0.5	2.84	0.20	39.2	3.1	22.0	7.5	3.8
N ₂₄₀ F _{LC} 302	ID	0.328	0.362	2.68	0.421	0.0	25.5	74.5	0.0	3.04	-0.65	17.1	9.8	17.2	5.4	2.8
N ₂₄₀ F _{LC} 338	LC	0.397	0.117	2.72	0.515	0.0	100.0	0.0	0.0	2.88	0.24	39.2	3.0	21.6	7.1	3.7
N ₂₈₀ F _{LC} 302	ID	0.354	0.378	2.29	0.385	0.0	10.9	89.1	0.0	2.85	-1.00	14.5	6.3	14.7	7.2	2.9
N ₂₈₀ F _{LC} 338	LC	0.408	0.118	2.58	0.502	0.0	100.0	0.0	0.0	2.82	0.22	40.1	3.0	21.9	7.6	3.9
N ₃₂₀ F _{LC} 302	ID	0.374	0.409	2.35	0.417	0.0	9.4	90.6	0.0	2.75	-1.25	10.3	3.6	11.4	4.7	2.4
N ₃₂₀ F _{LC} 338	LC	0.419	0.107	2.52	0.503	0.0	100.0	0.0	0.0	2.77	0.20	40.7	4.8	21.9	7.6	4.0
N ₃₆₀ F _{GL} 302	GL	0.235	0.315	3.87	0.433	100.0	0.0	0.0	0.0	4.22	0.39	23.0	2.7	7.2	21.8	3.2
N ₃₆₀ F _{GL} 338	LC	0.425	0.103	2.43	0.489	0.7	99.0	0.0	0.3	2.75	0.15	40.0	3.2	22.0	7.1	3.7
N ₃₆₀ F _{LC} 302	ID	0.373	0.419	2.21	0.393	0.0	10.4	89.6	0.0	2.72	-1.28	9.9	2.6	13.5	4.4	2.3
N ₃₆₀ F _{LC} 338	LC	0.431	0.103	2.40	0.490	0.0	100.0	0.0	0.0	2.72	0.19	41.4	3.6	22.8	7.4	3.8
N ₄₀₀ F _{GL} 302	GL	0.239	0.337	4.03	0.458	100.0	0.0	0.0	0.0	4.13	0.29	21.2	2.3	6.8	18.2	4.2
N ₄₀₀ F _{GL} 338	LC	0.444	0.100	2.63	0.558	0.6	99.1	0.0	0.3	2.67	0.38	46.4	4.4	25.1	8.0	4.1
N ₄₀₀ F _{LC} 302	ID	0.372	0.416	2.30	0.408	0.0	35.4	64.6	0.0	2.75	-1.21	10.6	2.8	15.6	4.6	2.4
N ₄₀₀ F _{LC} 338	LC	0.439	0.090	2.43	0.508	0.0	100.0	0.0	0.0	2.69	0.16	41.7	3.3	22.5	7.1	3.8
N ₄₄₀ F _{GL} 302	GL	0.235	0.329	4.00	0.449	100.0	0.0	0.0	0.0	4.21	0.39	22.4	3.3	6.9	21.0	4.2
N ₄₄₀ F _{GL} 338	LC	0.439	0.099	2.41	0.502	0.7	99.1	0.0	0.2	2.69	0.19	42.1	3.2	23.0	7.7	3.9
N ₄₄₀ F _{LC} 302	ID	0.353	0.382	2.25	0.378	0.0	20.7	79.3	0.0	2.87	-0.96	14.4	6.3	16.2	6.0	2.8
N ₄₄₀ F _{LC} 338	LC	0.444	0.092	2.45	0.516	0.0	100.0	0.0	0.0	2.66	0.21	43.2	3.6	23.5	7.7	3.9
N ₄₈₀ F _{GL} 302	GL	0.234	0.322	4.02	0.449	100.0	0.0	0.0	0.0	4.20	0.36	22.1	3.0	7.1	20.6	4.0
N ₄₈₀ F _{GL} 338	LC	0.447	0.104	2.42	0.516	0.3	99.5	0.0	0.2	2.68	0.18	42.2	3.7	22.9	7.5	3.8
N ₄₈₀ F _{LC} 302	ID	0.373	0.412	2.29	0.407	0.0	16.3	83.7	0.0	2.78	-1.18	10.6	2.4	16.2	4.6	2.4
N ₄₈₀ F _{LC} 338	LC	0.444	0.080	2.52	0.534	0.0	100.0	0.0	0.0	2.64	0.41	47.6	3.6	25.8	7.9	3.9

thickness of the bilayer. Similar considerations apply to the influence of temperature, which affects other properties of the LC phase in large part via a slight lateral expansion of the bilayer (in addition to the direct effect of increased thermal motion).

For the GL phase, the structural and dynamic parameters are essentially independent of the MET concentration as observed previously [81], with the possible exception of the collective azimuthal tilt angle Θ (see further below). However, for the ID phase, a_{xy} noticeably increases with the MET concentration. Interestingly, the correlation between this and the other parameters is different from that observed in the LC phase. Here, the increase in a_{xy} correlates with an increase (rather than a decrease) in S_{chn} , a decrease (rather than an increase) in θ and nearly no effect on d_z , v_{xyd} and D_{xy} . Note also that the value of g , which is negative in the ID phase, tendentially decreases with increasing a_{xy} , suggesting a slight increase in the degree of interpenetration of the two leaflets. The above trends are visible up to $n_M = 280$ (about 10 M), and tend to level off thereafter.

A possible interpretation of the above trends is the following. In the absence of interdigititation, the effective (solvated) headgroup cross-section is typically too large for the effective all-*trans* tail

cross-section, and a potential tail-packing deficit is alleviated by single-lipid (LC) or collective (GL) tilting [60]. In the LC phase, the single-lipid tilting (kinking) is associated with disorder and fluidity, so that a MET-induced increase in a_{xy} further enhances these properties. At a MET concentration just above c_{rev} interdigititation occurs, doubling the effective tail cross-section. Now the imbalance is reversed in direction, and it is the effective tail cross-section that is slightly too large for the effective headgroup cross-section, promoting an incomplete leaflet interpenetration and some extent of disorder in the tail segments closest to the headgroups. In this case, further increasing c_M (up to about 10 M) reduces the imbalance via an increase in a_{xy} , now promoting deeper interpenetration, tighter packing and increased ordering, opposite to the trend observed in the LC phase.

Two parameters of special interest are v_{xyd} and Θ . The volume per lipid v_{xyd} evidences relative changes of small magnitudes compared to those of a_{xy} and d_z , due to a partial cancellation in the variations of these two anti-correlated parameters within their product. Assuming an equivalent volume of 16 methylene groups per chain, the corresponding effective volumes per methylene group within the bilayer interior are about 0.030 (LC),

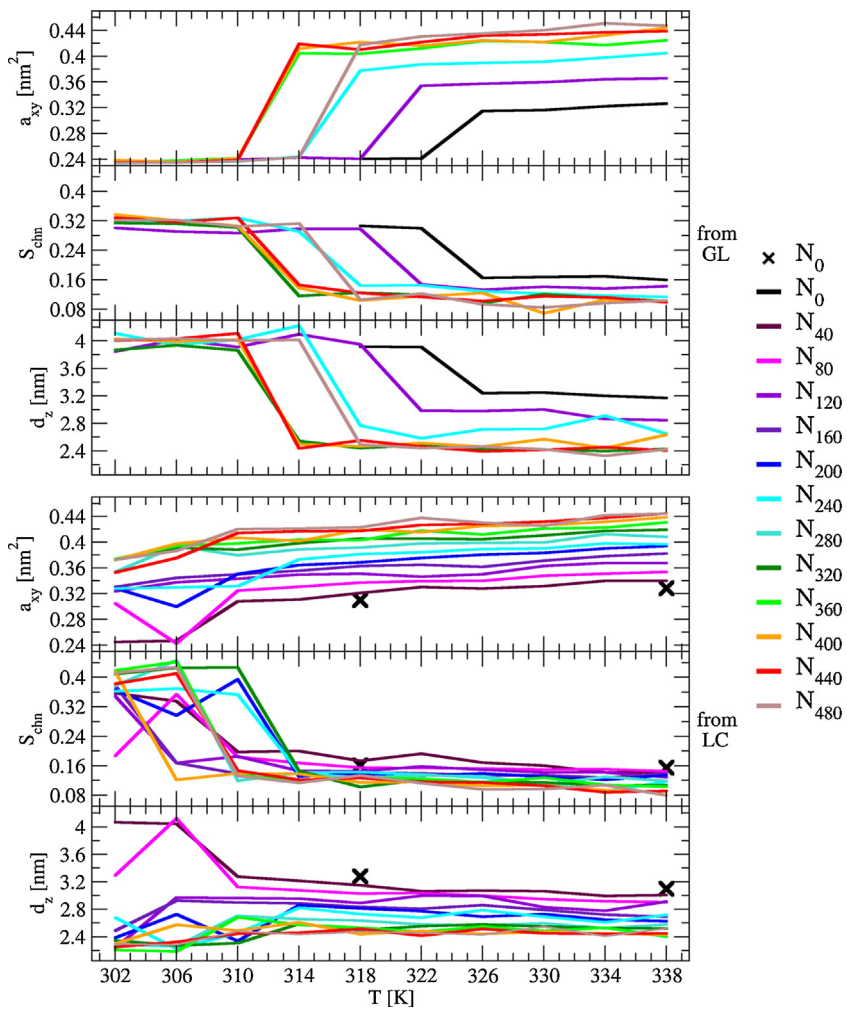


Fig. 5. Temperature dependence of the bilayer structural parameters for the entire set of simulations. Shown are the values of the area per lipid a_{xy} , the chain-averaged order parameter S_{chm} and the bilayer thickness d_z for the different simulations starting either from a structure appropriate for the GL phase (upper three panels) or LC phase (lower three panels) and carried out for 180 ns at different temperatures T . The different MET contents are distinguished by different colors. Note that for system N_0 , only two simulations were started from the LC phase at 318 and 338 K indicated by crosses (\times). The data is averaged over the last 24 ns of the simulation. The simulation labels and conditions are summarized in Table 1. (For interpretation of the references to color in this figure legend, the reader is referred to the web version of the article.)

0.028 (GL) and 0.025 (ID) nm³. The former and latter values are identical to the corresponding group increments for liquid and solid alkanes, respectively [81,112], the GL value being intermediate. This suggests that the phase changes are accompanied by a relatively limited change in the effective packing density of the lipid atoms within the bilayer, but a much more pronounced change in the packing anisotropy (area per lipid vs. bilayer thickness). Still, a slight increase in the packing density from LC to GL and from GL to ID represents an important second-order correction. In contrast, the effects of MET concentration and temperature are essentially insignificant, unless they induce a phase change. The collective tilt angle Θ is also essentially independent of c_M , presenting values of about 7.5° (LC), 10–25° (GL; with a significant variation across systems) and 5–10° (ID), indicating that this parameter is defined exclusively by the phase. The value is high only for GL, which presents a significant collective tilt. For the LC phase, the single-lipid tilt angles are the highest, but are randomly oriented across lipids, resulting in a low collective value. The lowest value is observed for the ID phase, where optimal packing is reached via interdigitation, so that tilting (single-lipid as well as collective) is no longer necessary [60].

The H-bonding properties are displayed in Fig. 7 (numerical values in Suppl. Mat. Table S.1). Based on Table 2, the left bar in each pair characterizes a GL phase (bottom panel for $n_M = 40$, entire top

panel) or an ID phase (bottom panel except $n_M = 0, 40$ and 80), whereas the right bar always characterizes a LC phase (so does the left bar for $n_M = 0$ or 80 in the bottom panel).

The occurrence of inter-layer lipid-lipid H-bonds ($2n_L^{-1}N_{LL}^{inter}$), i.e. between opposite leaflets across periodic boundaries, is very limited and essentially not visible on the scale of the figure (fraction of at most 0.06 in simulation $N_{120}F_{LC}302$). These H-bonds occur marginally in the ID and LC phases, and are essentially absent in the GL phase. The occurrence of intra-layer lipid-lipid H-bonds ($2n_L^{-1}N_{LL}^{intra}$) is about 2.0 per lipid for the GL phase, 1.5 for the ID phase and 1.0–1.5 for the LC phase, where the number decreases with increasing MET content. The higher occurrence in the GL compared to the ID and LC phases can easily be rationalized based on the higher area per lipid in the latter phases [57]. The occurrence of lipid-water H-bonds ($n_L^{-1}N_{LW}$) is about 1.3–2.3 per lipid for the GL phase, 1.9–2.4 per lipid for the ID phase and 2.0–2.8 for the LC phase. The lower occurrence in the GL compared to the ID and LC phases can again easily be rationalized based on the larger area per lipid (increased exposure of the headgroups to the solvent) in the latter phases. An increasing MET content reduces the occurrences of these H-bonds, introducing new lipid-MET H-bonds ($n_L^{-1}N_{LM}$) in all phases, their number increasing upon increasing the MET-to-water ratio in the system. This concentration-dependent replacement of lipid–water by lipid–MET H-bonds was observed

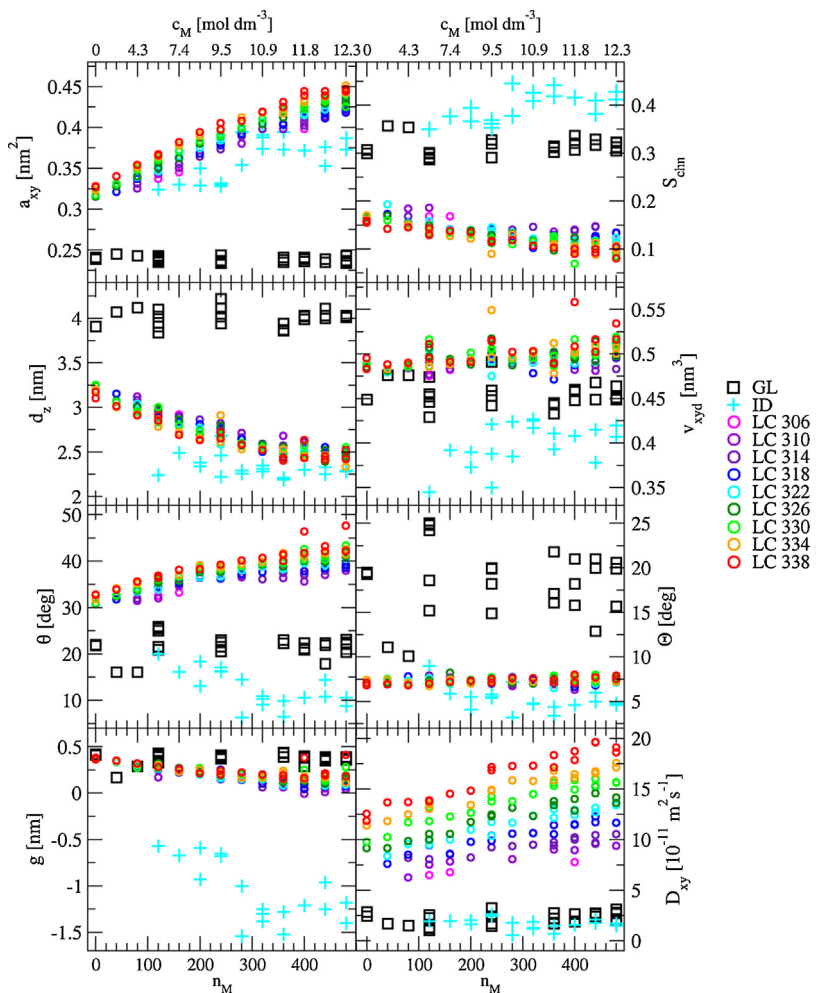


Fig. 6. Dependence of the structural parameters on the MET concentration for the entire set of simulations. Shown are correlations between the number n_M of MET molecules in the system (the corresponding molar concentration c_M is also indicated at the top) and the area per lipid a_{xy} , the chain-averaged order parameter S_{cha} , the bilayer thickness d_z , the volume per lipid v_{xyd} , the average single-lipid tilt angle θ , the collective tilt angle Θ , the bottom-to-top distance between the planes of the terminal methyl groups g , and the diffusion coefficient D_{xy} . The different simulations vary by the final phase (GL, LC, ID; UN not shown), represented by different symbols. For simulations with LC as final phase, different temperatures T are also distinguished by different colors. The values are averaged over the last 24 ns of the simulations. The simulation labels and conditions are summarized in Table 1.

experimentally in infrared measurements for DPPC and methanol, ethanol, and *n*-butanol [32]. However, it has been suggested that although the number of MET–lipid interactions increases with increasing MET content, their strength (calculated as a preferential binding parameter of the alcohol–lipid interaction based on vapor pressure experiments) decreases [113]. Considering the fractions f_{EW} and f_{EM} of lipid–water and lipid–MET H-bonds involving the ester as opposed to the glycerol moiety of the lipids (Suppl. Mat. Table S.1), it is seen that water and MET present a large overlap with the glycerol region and penetrate the bilayer up to the ester region, especially in the LC phase. A more detailed interpretation of these observations is given in Refs. [53,81].

When considering the sum N_L^{tot} of the inter-layer lipid–lipid, intra-layer lipid–lipid, lipid–water and lipid–MET H-bonds per lipid, this number remains essentially constant for all the systems considered, with a value close to four (4.1–4.3). With increasing MET content, one essentially observes a suppression of inter-layer lipid–lipid H-bonds, a decrease in intra-layer lipid–lipid H-bonds and a partial substitution of lipid–water by lipid–MET H-bonds. Such a nearly quantitative compensation effect is in the agreement with a H-bond conservation principle [81] and has been observed previously for this system [54,57,81] as well as in different contexts [47,53,55,114,115], i.e. a change in the environmental conditions

induces a mere redistribution of the four lipid–environment H-bonds among the different species present in the system. A H-bond conservation principle similar to that suggested for the lipid headgroups [81] also holds for the MET and water molecules. The total number of H-bonds per MET and water molecule (N_M^{tot} and N_W^{tot}) is close to 2.2 (range 2.1–2.4) and 3.0 (range 3.0–3.3), respectively, for all systems. The value for water is comparable to the corresponding numbers of about 3.3 or 3.2 for bulk water at 318 and 338 K, respectively [81].

Differences between water and MET are also seen in the extent of H-bonded bridging, i.e. the number of water molecules n_W^m and MET molecules n_M^m being simultaneously H-bonded with a given number m of lipid molecules, as illustrated in Fig. 8 (numerical values in Suppl. Mat. Table S.2). Here again, the left bar in each pair characterizes a GL phase (bottom panel for $n_M = 40$, entire top panel) or an ID phase (bottom panel except $n_M = 0, 40$ and 80), whereas the right bar always characterizes a LC phase (so does the left bar for $n_M = 0$ or 80 in the bottom panel).

The quantities $n_L^{-1}(n_W - n_W^0)$ and $n_L^{-1}(n_M - n_M^0)$ (total bar height) represent average numbers of water and MET molecules, respectively, H-bonded to the bilayer on a per-lipid basis. For all systems, these numbers are systematically lowest for the GL phase, intermediate for the ID phase and highest for the LC phase. The

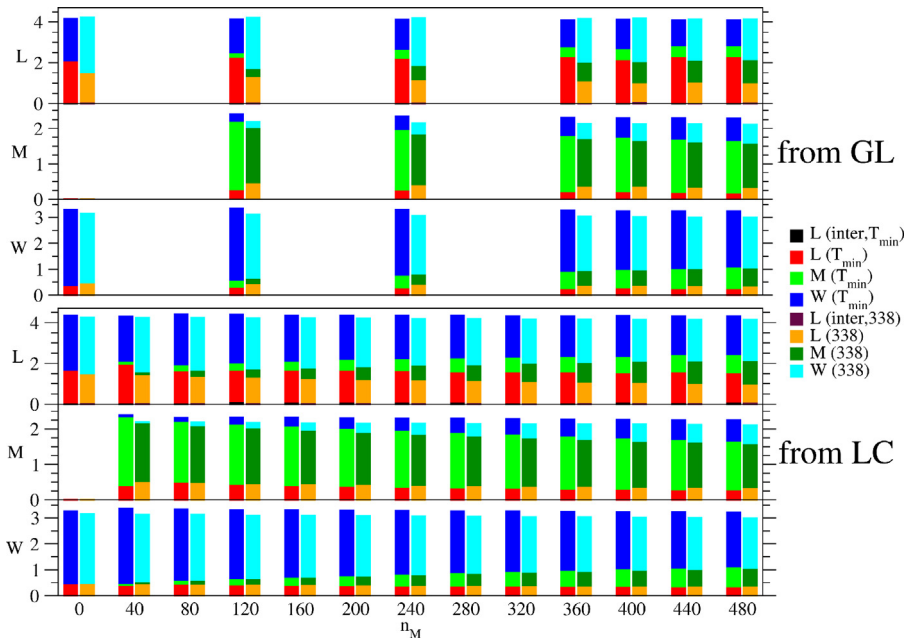


Fig. 7. Average hydrogen bonding (H-bonding) properties for a subset of simulations at the highest and lowest temperatures. This subset encompasses the simulations started from a structure appropriate for either the GL phase (top panel) or the LC phase (bottom panel) at reference temperatures T_{min} of 318 K (system N_0) or 302 K (all other systems) and 338 K, for the different MET contents n_M . The bars show the total numbers of H-bonds per lipid N_L^{tot} (top panels L), per MET N_M^{tot} (middle panels M) and per water N_W^{tot} (bottom panels W). The different colors within the bars correspond to a partitioning in terms of the second species involved in these H-bonds (L, M or W), also distinguishing for the lipid–lipid interactions between inter-layer and intra-layer with a different color. Based on the total numbers of H-bonds between the species, this partitioning is given by $N_L^{tot} = n_L^{-1}(2N_{LL}^{inter} + 2N_{LL}^{intra} + N_{LM} + N_{LW})$, $N_M^{tot} = n_M^{-1}(N_{LM} + 2N_{MM} + N_{MW})$ and $N_W^{tot} = n_W^{-1}(N_{LW} + N_{MW} + 2N_{WW})$. The data is averaged over the last 24 ns of the simulation. The simulation labels and conditions are summarized in Table 1. The numerical values corresponding to this figure are provided in Table S.1 of the Suppl. Mat. document. Corresponding data for the entire set of 239 simulations can be also found in Tables S.5 and S.11. (For interpretation of the references to color in this figure legend, the reader is referred to the web version of the article.)

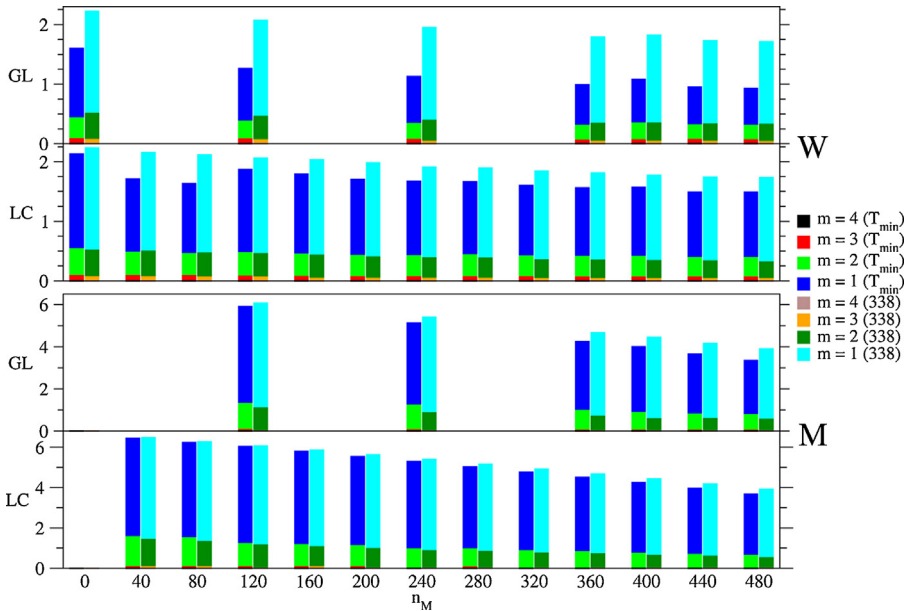


Fig. 8. Extent of H-bonded bridging of the lipids calculated from a subset of simulations at the highest and lowest temperatures. This subset encompasses the simulations started from a structure appropriate for either the GL phase or the LC phase at reference temperatures T_{min} of 318 K (system N_0) or 302 K (all other systems) and 338 K, for the different MET contents n_M . The quantities n_W^m and n_M^m with $m = 0, \dots, 4$ represent the numbers of water and MET molecules, respectively, being simultaneously H-bonded (as acceptor or as donor, and possibly via more than one H-bond) to a given number m of lipid molecules. These numbers add up to the total number of water molecules n_W and MET molecules n_M , respectively, in the simulated system. The bars show the numbers of lipid-bound water molecules $n_L^{-1}(n_W - n_W^0)$ (top graph W) and MET molecules $n_L^{-1}(n_M - n_M^0)$ (bottom graph M) on a per-lipid basis. The different colors within the bars correspond to a partitioning in terms of the fraction of these bound molecules being simultaneously H-bonded to given number m of lipid molecules. This partitioning is given by $n_L^{-1}(n_W - n_W^0) = n_L^{-1}(n_W^1 + n_W^2 + n_W^3 + n_W^4)$ and $n_L^{-1}(n_M - n_M^0) = n_L^{-1}(n_M^1 + n_M^2 + n_M^3 + n_M^4)$. The data is averaged over the last 24 ns of the simulations. The simulation labels and conditions are summarized in Table 1. The numerical values corresponding to this figure are provided in Table S.2 of the Suppl. Mat. document. Corresponding data for the entire set of 239 simulations can also be found in Tables S.6 and S.12. (For interpretation of the references to color in this figure legend, the reader is referred to the web version of the article.)

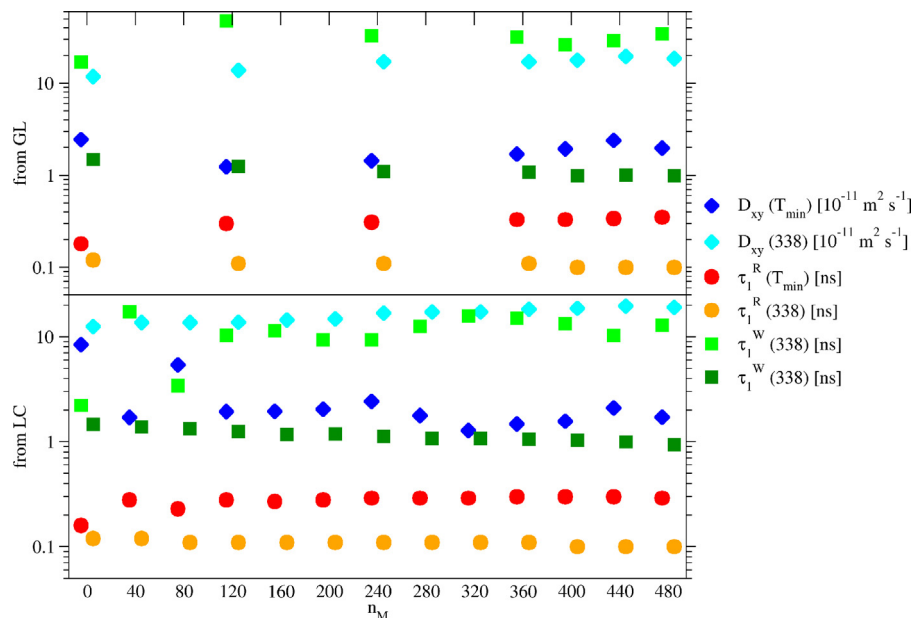


Fig. 9. Average dynamic properties for a subset of simulations at the highest and lowest temperatures. This subset encompasses the simulations started from a structure appropriate for either the GL phase (top panel) or the LC phase (bottom panel) at reference temperatures T_{min} of 318 K (system N₀) or 302 K (all other systems) and 338 K, for the different MET contents n_M . The quantities displayed are the lipid lateral diffusion coefficient D_{xy} , the first relaxation time τ_l^R for the lipid rotational motion, and the first relaxation time τ_l^W for the lipid and wobbling motion. The values are averaged over the last 24 ns of the simulations. The simulation labels and conditions are summarized in Table 1. The numerical values corresponding to this figure are provided in Table S.3 of the Suppl. Mat. document. Corresponding data for the entire set of 239 simulations can also be found in Tables S.7 and S.13.

average number of H-bonded water and MET molecules are in the ranges 0.9–2.2 and 3.3–6.4, respectively, and decrease with increasing MET content.

The quantities $(n_W - n_W^o)^{-1} n_W^m$ and $(n_M - n_M^o)^{-1} n_M^m$ (fraction of the bar height covered by different color segments) represent fractions of these H-bonded water and MET molecules, respectively, forming simultaneously H-bonds with (*i.e.* bridging) m lipids. Considering the H-bonded water molecules, about 75% are H-bonded to a single lipid, about 20% to two lipids simultaneously,

and about 5% to three lipids simultaneously, irrespective of the phase. Upon increasing the MET concentration, water bridging is slightly enhanced in the GL phase and pronouncedly decreased in the LC phase, most likely due to the lateral expansion of the bilayer, while remaining essentially constant in the ID phase. For the bound MET molecules, H-bonding to more than two lipids simultaneously is scarce and overall less frequent in the LC and ID phases than in the GL phase. Upon increasing the MET concentration, MET bridging is essentially unchanged in the ID and GL phases and

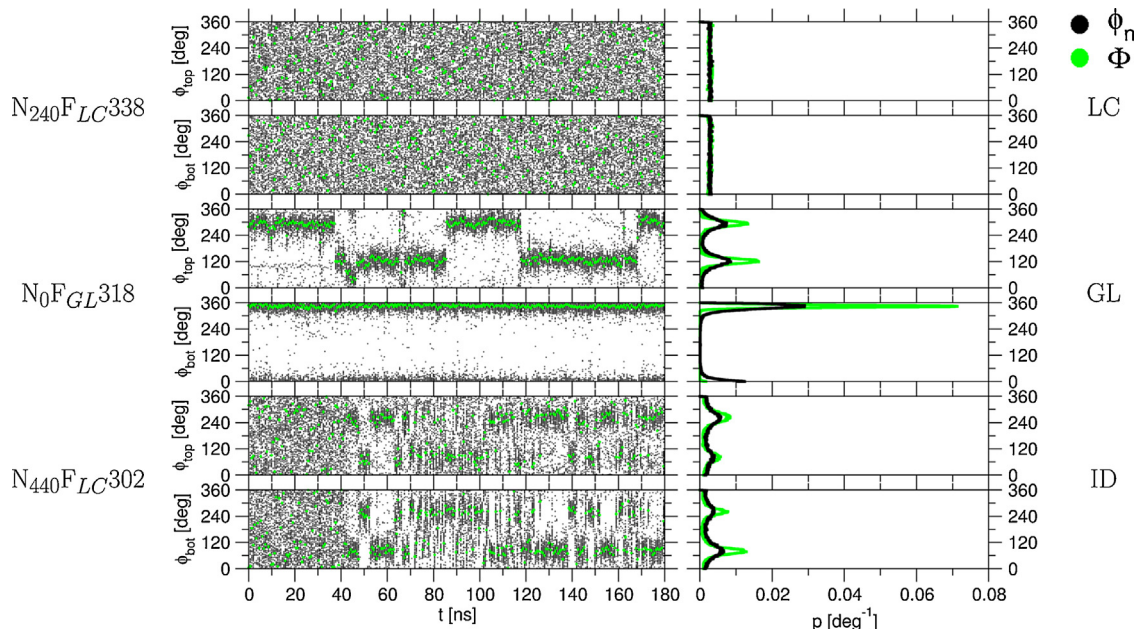


Fig. 10. Illustrative time series of the azimuthal tilt angles and corresponding probability distributions for the three phases occurring in the simulations. Shown are the azimuthal tilt angles ϕ_n ($n=1-128$) for each individual lipid, distinguishing bottom (bot) and top (top) leaflets, and the corresponding collective angle Φ over the entire 180 ns simulation time for simulations illustrative of the GL (top), LC (middle) and ID (bottom, after a transition from LC at 40 ns) phases. The associated normalized probability distributions p are also shown. The time step between individual data points is 1 ps. The simulation labels and conditions are summarized in Table 1.

Table 4

Probabilities of collective azimuthal tilt-angle values calculated from a subset of simulations corresponding to low-temperature equilibrium conditions for the GL phase. This subset encompasses the simulations started from a structure appropriate for either the GL phase or the LC phase at reference temperatures of 318 K (system N_0) or 302 K (all other systems), for the different MET contents n_M . Only systems which are in the GL phase for more than 10% of the simulation time are considered. The quantities reported are the percentage ρ_{GL} of configurations in the GL phase over the 180 ns simulation time and the percentage of these GL configurations with the collective azimuthal tilt angles Φ_{bot} and Φ_{top} for the bottom and top leaflets, respectively, belonging to the specific intervals ($\pm 15^\circ$ for the bottom layer, or $\pm 120^\circ$ or $\pm 60^\circ$ for the top layer, within ranges of $\pm 15^\circ$). The simulation labels and conditions are summarized in Table 1. The data for the entire set of simulations with SEMI and FULL pressure coupling can be found in Tables S.8 and S.14, respectively, of the Suppl. Mat. document.

Simulation	ρ_{GL} (%)	P_{+15}^{bot} (%)	P_{-15}^{bot} (%)	P_{+60}^{top} (%)	P_{+120}^{top} (%)	P_{-120}^{top} (%)	P_{-60}^{top} (%)
$N_0 F_{GL} 318$	100.0	0.6	98.9	1.4	37.5	1.7	30.1
$N_{40} F_{LC} 302$	51.7	3.4	2.6	1.3	2.2	40.3	7.1
$N_{120} F_{GL} 302$	100.0	0.0	100.0	0.0	58.4	0.0	0.0
$N_{240} F_{GL} 302$	100.0	0.1	99.9	75.3	0.4	0.0	0.0
$N_{360} F_{GL} 302$	100.0	0.1	99.8	0.0	89.4	0.0	0.0
$N_{400} F_{GL} 302$	100.0	4.0	90.3	85.0	0.0	0.0	0.0
$N_{440} F_{GL} 302$	100.0	0.2	99.7	0.0	0.0	0.2	80.3
$N_{480} F_{GL} 302$	100.0	0.2	99.8	0.1	82.2	0.0	0.0

slightly decreased in the LC phase, both effects most likely due to the lateral expansion induced by the MET molecules. The slight loosening of the H-bond network (fewer water and MET molecules bound to more than one lipid) is in line with the observed decrease in the rigidity (shorter H-bond lifetimes) of the lipid hydration layer observed experimentally for ethanol with dimyristoylphosphatidylcholine lipid bilayers [11,116].

The dynamic properties are displayed in Fig. 9 (numerical values in Suppl. Mat. Table S3). The translational diffusion coefficient D_{xy} is systematically lower for the GL and ID phases compared to the LC phase. It increases with increasing MET content for the LC phase while remaining essentially constant for both the GL and ID phases. The first decay time τ_1^R for the rotational autocorrelation function, attributed to the rotation of a single lipid around its axis and associated with a low residual correlation (as expected for a vector that samples the accessible space isotropically), corresponds to a timescale of about 0.2–0.3 ns for the GL and ID phases and 0.1 ns for the LC phase. The first decay time τ_1^W for the wobbling autocorrelation function, attributed to the wobbling of a single lipid and associated with a high residual correlation (as expected for a vector that does not sample the accessible space isotropically), corresponds to a timescale of about 20–50 ns for the GL phase, 10–15 ns for the ID phase and 1–1.5 ns for the LC phase. The values for the ID phase are similar to those in the GL phase [81]. These trends can easily be rationalized [54,57] based on the lower extent of ordering of the LC compared to the GL and ID phases, but may also reflect in part the higher simulation temperature.

3.3. Tilt precession

Illustrative results for the time evolution of the single-lipid azimuthal tilt angles ϕ_n ($n = 1, \dots, 128$) are shown in Fig. 10, separately for the bottom and top leaflets. This angle represents, for each lipid in a given trajectory configuration, the angle between the projection of the lipid head-tail vector in the xy -plane (bilayer plane) and the x -axis (one edge of the simulation box). The three successive panels correspond to simulations $N_{240} F_{LC} 338$, $N_0 F_{GL} 318$ and $N_{440} F_{LC} 302$, respectively, sampling the LC, GL and ID phases, respectively (for $N_{440} F_{LC} 302$, the ID phase is sampled only after a LC \rightarrow ID transition at 40 ns). Similar figures have been presented and discussed previously in Ref. [60] (see Figs. 4 and 5 therein), and the present analysis focuses on more specific observations in the context of MET-containing systems and of the ID phase.

In the LC phase, the azimuthal tilt angles are essentially randomly distributed across the lipids at all time points, i.e. the tilting (kinking) of the individual lipids occur in arbitrary (isotropic) directions. This absence of correlation among the ϕ_n explains why the single-lipid apical tilt angle θ can be large (about 30–45°) while

the corresponding collective value Θ is small (about 7.5°) for this phase, as seen in Section 3.2. For this phase, a further examination of the probability distribution of the ϕ_n angles (or a corresponding averaging) makes no sense since these distributions are homogeneous.

In the GL phase, the single-lipid tilt angles ϕ_n are largely correlated across the lipids, with root-mean-square deviations on the order of 20° around time-dependent average values Φ . This high extent of correlation among the ϕ_n angles explains why the single-lipid apical tilt angle θ (about 15–25°) is about equal to the corresponding collective value Θ (about 10–25°) for this phase, as seen in Section 3.2. The preferred average values Φ are time-dependent, i.e. change on the 50–100 ns timescale [60] (precession). These preferred average values are also distinct for the bottom and top leaflets, and the precession motion almost exclusively concerns the top leaflet in the present simulations.

For the ID phase, a behavior similar to that of the LC phase was suggested in Ref. [60] on the basis of a limited set of simulations. This was reasonable considering that the single-lipid apical tilt angle θ is typically very small (about 10°), and the collective value Θ (about 5°) even smaller for this phase, as seen in Section 3.2. In this case, the projection of the single-lipid head-tail vectors in the xy -plane is very short, and its azimuthal orientation expected to be dictated by small random (and largely irrelevant) fluctuations. However, considering the present much larger set of simulations sampling the ID phase over relatively long time periods, a behavior similar to that of the GL phase is also sometimes observed instead. The preferred average values Φ are also time-dependent, but tend to change on a faster 5–10 ns timescale (precession). In addition, in contrast to the GL behavior, these preferred values are the same for the bottom and top leaflets, and vary in a correlated fashion. Correlated Φ changes between the two leaflets are expected in view of the constraint of interdigitation, i.e. if the bottom leaflet tilts in one direction, the opposite leaflet is expected to tilt in an opposite direction ($\Phi_{top} - \Phi_{bot} = 180^\circ$, taking the Φ periodicity into account). The bottom panel of Fig. 10 presents a typical situation of this GL-like behavior (see Figure 4 bottom right panel in Ref. [60] for an example of LC-like behavior).

Tables 4 and 5 report the populations of the main preferred states of the collective Φ angle in the GL and ID phases based on the 40 simulations with SEMI pressure coupling corresponding to the lowest (318 K for N_0 and 302 K for all other systems) and the highest (338 K) temperatures considered at each MET content, considering separately values for the bottom and top leaflets, Φ_{bot} and Φ_{top} , respectively. The corresponding averages for the entire set of 188 simulations with SEMI pressure coupling can be found in Suppl. Mat. Tables S.8 and S.9. The statistics is based on the entire 180 ns simulation period, but restricted to the trajectory configurations assigned to the specific phase (GL or ID) using the

Table 5 Probabilities of collective azimuthal tilt-angle values calculated from a subset of simulations corresponding to low-temperature equilibrium conditions for the ID phase. This subset encompasses the simulations started from a structure appropriate for the LC phase at a reference temperature of 302 K, for the different MET contents n_M . Only systems which are in the ID phase for more than 10% of the simulation time are considered. The quantities reported are the percentage ρ_{ID} of configurations in the ID phase over the 180 ns simulation time and the percentage of these ID configurations with the collective azimuthal tilt angles Φ_{bot} and Φ_{top} for the bottom and top leaflets, respectively, belonging to the specific intervals $(0^\circ, \pm 60^\circ, \pm 90^\circ, \pm 120^\circ, \pm 180^\circ)$ within ranges of $\pm 15^\circ$. The simulation labels and conditions are summarized in Table 1. The data for the entire set of simulations with SEMI and FULL pressure coupling can be found in Tables S.9 and S.15, respectively, of the Suppl. Mat. document.

Simulation	$\rho_{\text{ID}} (\%)$	$P_0^{\text{bot}} (\%)$	$P_{+60}^{\text{bot}} (\%)$	$P_{-60}^{\text{bot}} (\%)$	$P_{180}^{\text{bot}} (\%)$	$P_{+20}^{\text{bot}} (\%)$	$P_{-90}^{\text{bot}} (\%)$	$P_{+120}^{\text{bot}} (\%)$	$P_0^{\text{top}} (\%)$	$P_{+60}^{\text{top}} (\%)$	$P_{-60}^{\text{top}} (\%)$	$P_{180}^{\text{top}} (\%)$	$P_{+20}^{\text{top}} (\%)$	$P_{-90}^{\text{top}} (\%)$	$P_{+120}^{\text{top}} (\%)$		
N ₁₂₀ F _C 302	53.5	3.5	3.6	14.5	17.8	2.3	5.2	16.0	19.5	0.6	1.3	21.5	27.8	0.5	0.7	15.2	27.5
N ₁₆₀ F _C 302	16.9	6.6	3.8	5.7	16.5	3.9	3.8	8.8	17.1	15.9	7.2	10.2	11.5	4.8	2.2	2.2	5.5
N ₂₀₀ F _C 302	46.5	5.1	3.1	7.1	19.5	5.7	2.5	4.5	12.8	11.7	6.1	9.0	10.7	3.7	7.2	7.2	13.2
N ₂₄₀ F _C 302	74.5	4.2	13.8	11.3	6.8	8.5	13.8	8.1	4.2	6.2	17.3	6.5	3.3	4.9	15.3	6.2	3.5
N ₂₈₀ F _C 302	89.1	19.0	2.4	2.0	4.0	20.8	2.9	2.8	4.4	27.9	1.8	1.8	3.5	23.6	1.3	1.0	2.1
N ₃₂₀ F _C 302	90.6	17.1	5.2	4.2	5.0	14.1	5.3	4.4	5.1	16.2	4.4	3.6	4.3	19.9	4.3	3.3	4.1
N ₃₆₀ F _C 302	89.6	17.7	4.9	3.8	4.5	17.4	4.3	2.9	3.9	15.7	4.5	3.5	5.0	19.2	4.6	3.7	4.4
N ₄₀₀ F _C 302	64.6	3.8	12.1	20.3	10.3	3.2	7.6	14.2	9.5	5.1	10.0	12.8	7.3	3.3	9.3	19.0	13.2
N ₄₄₀ F _C 302	79.3	1.3	16.8	33.1	5.7	1.2	10.9	19.3	4.0	1.7	10.4	16.5	5.8	2.4	15.5	24.6	10.2
N ₄₈₀ F _C 302	83.7	3.9	9.5	14.6	4.3	10.1	17.9	10.5	4.0	12.3	19.8	9.3	2.8	8.4	16.5	9.4	

phase-assignment descriptor. The corresponding trajectory fraction, ρ_{GL} or ρ_{ID} , is also indicated.

As previously observed [60], for the GL phase, the bottom layer predominantly samples Φ values around $\pm 15^\circ$ while the top layer samples values close to $\pm 60^\circ$ or $\pm 120^\circ$. The preference of one leaflet for an azimuthal tilt angle of close to 0° (*i.e.* tilting essentially in the direction of the x -axis of the computational box) is almost certainly an artifact of the periodic boundary conditions imposed to the simulated system. Because the two leaflets of the bilayer are racemic mixtures of the *R* and *S* enantiomers of GMP, there is no topological distinction between bottom and top leaflets and between $-\Phi$ and $+\Phi$ values. The observed asymmetries (different populations for $-\Phi$ and $+\Phi$ states, alignment of the bottom rather than the top leaflet along the x -axis, preference for the x - over the y -axis) are thus coincidental, *i.e.* related to the arbitrary choice of an initial configuration and the finite timescale of the simulations. Making abstraction of these coincidental asymmetries, the simulations suggest a preference for relative tilt directions of the two leaflets at about $\pm 60^\circ$ or $\pm 120^\circ$ from each other in the GL phase of a racemic $2 \times 8 \times 8$ GMP bilayer patch, with a precession time of about 50–100 ns in this angle.

In the ID phase, both the bottom and top leaflets predominantly sample Φ values around 0° , $\pm 60^\circ$, $\pm 90^\circ$, $\pm 120^\circ$ and 180° . As mentioned above, the tilt directions of the top and bottom leaflets occur in opposite directions ($\Phi_{\text{top}} - \Phi_{\text{bot}} = 180^\circ$, taking the Φ periodicity into account). Thus, here, all the observed preferences (specific Φ states) are related to the artificial periodicity of the simulated system. Making abstraction of this artificial anisotropy, the simulations suggest a preference for relative tilt directions of the two leaflets at about 180° from each other in the ID phase of a racemic $2 \times 8 \times 8$ GMP bilayer patch, with a precession time of about 5–10 ns for the corresponding direction.

3.4. Pressure-coupling scheme

For the systems at three different MET concentrations ($n_M = 120$, 240 or 480), the simulations from the main set were repeated using a fully-anisotropic (FULL) pressure-coupling scheme, instead of the usual semi-anisotropic (SEMI) scheme. In the SEMI scheme, the x - and y -edges of the computational box (bilayer plane) are constrained to constant proportions when applying the pressure coupling (barostat) based on a joint pressure P_{xy} . In the present simulations, these proportions are those of a square (identical x - and y -edges). In the FULL scheme, the scaling is performed separately for the two edges based on the corresponding pressures P_x and P_y , respectively, so that these proportions can change. Considering the box edge lengths in the different simulations, reported in suppl. Mat. Table S.16, the ratio of the x - to y -edge length is about one for the GL phase, but varies in a range of about 0.6–2.3 for the LC phase. In both cases, the z -edge of the box (bilayer normal) is scaled independently based on the corresponding pressure P_z .

The average values of key properties calculated over the last 24 ns of these 52 simulations are reported in Table S.10 (structural properties and phase assignment), Tables S.11 and S.12 (H-bonding properties), Table S.13 (dynamic properties) and Tables S.14 and S.15 (tilt-angle properties). The comparison of the phase structural and dynamic properties corresponding to the simulations with SEMI and FULL pressure coupling do not reveal dramatic differences, as was already suggested in Ref. [65] in the context of DPPC simulations. This data will not be discussed in details here, the main goal of these simulations being to assess the influence of the pressure-coupling scheme on the estimated transition temperatures.

To this purpose, the occurrence of phase transitions for these simulations are listed in Table 6 and the values of a_{xy} , S_{chn} and d_z are displayed as a function of temperature for the different MET

Table 6

Occurrence of a phase transition for a subset of simulations. The simulations were started from a structure appropriate for the GL phase or the LC phase and carried out during 180 ns with semi-anisotropic (SEMI) pressure coupling or fully-anisotropic (FULL) pressure coupling. They differ in terms of the number n_M of MET molecules and the reference temperature T . A minus (–) indicates the absence of a transition, a cross (×) the presence of a GL → LC transition and a circle (○) the presence of a LC → ID transition. The simulation labels and conditions are summarized in Table 1.

Initial phase	$T[K]$	n_M		240		480		
		120		FULL	SEMI	FULL	SEMI	
		FULL	SEMI	FULL	SEMI	FULL	SEMI	
GL	338	×	×	×	×	×	×	×
GL	334	×	×	×	×	×	×	×
GL	330	×	×	×	×	×	×	×
GL	326	×	×	×	×	×	×	×
GL	322	×	×	×	×	×	×	×
GL	318	–	–	×	×	×	×	×
GL	314	–	–	–	–	–	–	–
GL	310	–	–	–	–	–	–	–
GL	306	–	–	–	–	–	–	–
GL	302	–	–	–	–	–	–	–
LC	338	–	–	–	–	–	–	–
LC	334	–	–	–	–	–	–	–
LC	330	–	–	–	–	–	–	–
LC	326	–	–	–	–	–	–	–
LC	322	–	–	–	–	–	–	–
LC	318	–	–	–	–	–	–	–
LC	314	–	–	–	–	–	–	–
LC	310	–	–	○	○	○	○	–
LC	306	○	–	○	○	○	○	○
LC	302	○	○	○	○	○	○	○

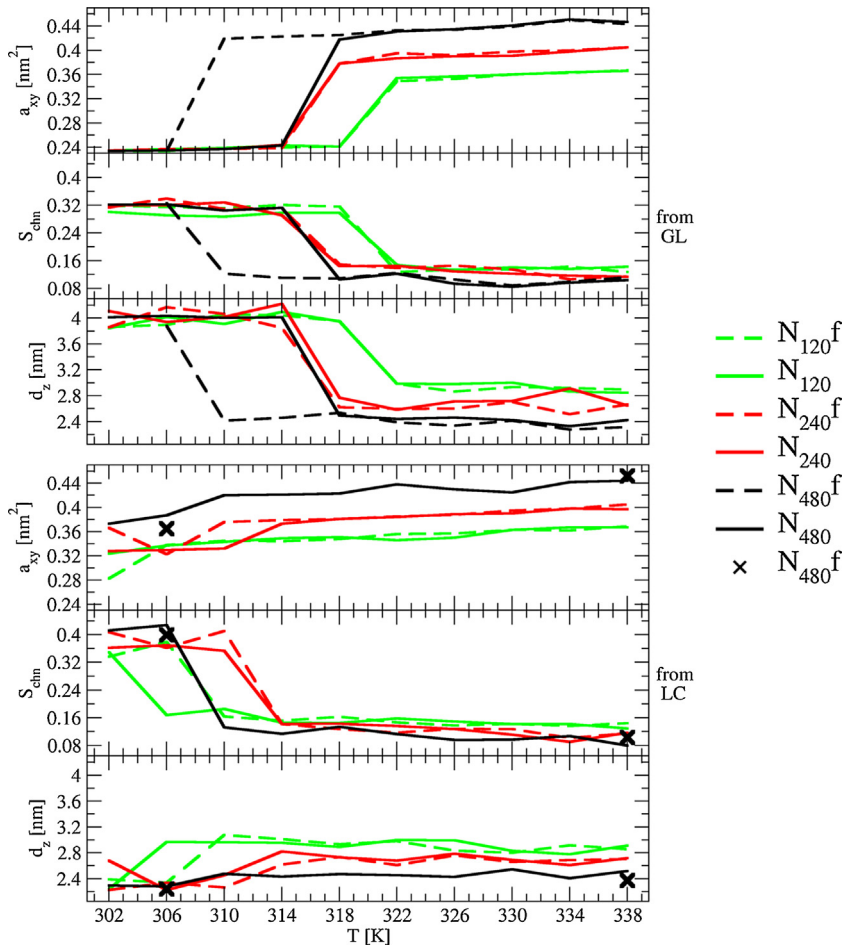


Fig. 11. Temperature dependence of the bilayer structural parameters for the pressure scaling comparison. Shown are the values of the area per lipid a_{xy} , the chain-averaged order parameter $S_{d\text{lm}}$ and the bilayer thickness d_z for the different simulations starting either from a structure appropriate for the GL phase (upper three panels) or LC phase (lower three panels) and carried out for 180 ns at different temperatures T . The different MET contents are distinguished by different colors. The dashed lines correspond to systems with semi-anisotropic pressure scaling (SEMI), and the solid lines to systems with fully-anisotropic pressure scaling (FULL). Note that for system $N_{480}T_f$, only two simulations were started from the LC phase at 306 and 338 K indicated by crosses (×). The data is averaged over the last 24 ns of the simulation. The simulation labels and conditions are summarized in Table 1. (For interpretation of the references to color in this figure legend, the reader is referred to the web version of the article.)

concentrations in Fig. 11. For the GL → LC transitions, the change from SEMI to FULL coupling (compare Figs. 5 and 11, or Tables 2 and 6) has no influence on the temperature- and concentration-dependent behavior, except at the highest MET concentration ($n_M = 480$), where a decrease in T_m of about 8 K is observed. The LC → GL transition is not observed considering that the lowest MET concentration considered here is already above $c_{rev} = 5.2$ M. For the LC → ID transition, the change from SEMI to FULL has no influence on the temperature- and concentration-dependent behavior except at the lowest MET concentration ($n_M = 120$), where an increase in T_m of about 4 K is observed. Considering the discussion of Section 3.1 concerning the limited precision of T_m estimations based on single-event simulations, these small differences are probably not statistically significant. In principle, a limited increase in T_m from SEMI to FULL for transitions from ordered (GL or ID) phases to a less ordered (LC) phase could be expected, considering that the artificial constraint introduced on the xy-plane proportions are likely to have a more adverse influence on a structured (crystal-like) as opposed to a less structured (liquid-like) phase. However, it also appears that the release of this constraint in the GL phase does not lead to a significant relaxation of the box proportions in the present case (ratio of the box edge lengths remaining close to 1 in the GL phase with FULL coupling; see suppl. Mat. Table S.16).

4. Conclusion

The present study expands the initial results of previous simulations [81] investigating the effect of MET on the phase and phase-transition properties of GMP bilayers. More specifically, the goal was to shed more light on still open questions regarding the relative (meta)stabilities of the GL and ID phases, the kinetic reversibilities of the different transitions on the simulated timescale, the impact of hysteresis on the simulation results, and the correct interpretation of these results in terms of the biphasic effect. To this purpose, 196 additional simulations of a $2 \times 8 \times 8$ GMP bilayer patch at full hydration were undertaken considering MET concentrations c_M ranging from 0 to 12.3 M and temperatures T ranging from 302 to 338 K, the entire data set being analyzed on a common 180 ns timescale. Two side issues were also addressed concerning: (i) the possible occurrence of collective tilting in the ID phase, and the nature of the associated tilt-precession motions [60]; (ii) the influence of the pressure coupling scheme employed in the simulations, semi- or fully-anisotropic, on the simulation results.

The main results concerning the phase-transition properties are summarized in Fig. 4, including both raw and tentative hysteresis-corrected transition temperatures (top panel) along with a schematic phase diagram illustrating a possible interpretation of this data (bottom). For MET concentrations c_M below $c_{rev} = 5.2$ M, the GL phase is stable at low temperatures and the LC phase at high temperatures. Reversible LC ↔ GL transitions are observed, albeit with a significant hysteresis on the 180 ns timescale, and T_m decreases upon increasing c_M . For MET concentrations above c_{rev} , the ID phase is stable at low temperatures and the LC phase at high temperatures. Decreasing the temperature leads to LC → ID transitions, again with a significant hysteresis, and T_m increases upon increasing c_M (up to about 10 M, remaining essentially constant thereafter). In this regime, however, the simulations initiated from the GL phase and presenting GL → LC transitions upon increasing the temperature actually probe changes between two metastable phases in an area of the phase diagram where the ID phase is the stable one. This interpretation could be confirmed by performing additional simulations probing the ID → LC transition at $c_M > c_{rev}$ (work in progress).

The simulations lead to an estimate $c_{rev} = 5.2$ M for the biphasic reversal concentration of GMP in the presence of MET, larger than

the experimental value [30,36,111] of about 2.5 M for DPPC. Quantitative agreement is of course not expected considering that c_{rev} can vary widely depending on the nature of the alcohol, on the number and length of the lipid tails, and on the type of headgroup functionalization. On the other hand, the hysteresis-corrected estimate for T_m in the absence of MET at full hydration, about 320 K, compares very well with the experimental value [54,84] of 323 K.

The above interpretation of the simulation results is compatible with the expected features of the biphasic effect, even if this interpretation remains to be further validated by: (i) longer simulations to reduce the hysteresis ranges; (ii) simulation repeats to increase the statistical accuracy; (iii) additional simulations with $c_M > c_{rev}$ initiated from the ID phase. Work is currently in progress along these lines. Another possible direction for the reduction of hysteresis errors would be the application of a simulation scheme relying on replica exchange in temperature [117–121].

The analysis of the structural and dynamical properties reveals very different sensitivities and responses of the three phases to changes in c_M and T over the ranges considered. The properties of the GL phase are essentially insensitive to both c_M and T over its stability range (low c_M and low T). In contrast, the properties of the LC phase depend strongly on c_M and slightly on T over its stability range (high T), the trends upon increasing either of the two parameters being the same. Finally, the properties of the ID phase are moderately sensitive to c_M and essentially insensitive to T over its stability range (high c_M and low T).

Interestingly, however, the responses of the LC phase (strong) and the ID phase (moderate) to a change in c_M are different. In both cases, an increase in c_M leads to an increase in a_{xy} , due to the intercalation of additional MET molecules between the lipid headgroups. For the LC phase, this increase in a_{xy} promotes a decrease in the bilayer thickness, and an increase in the extent of single-lipid tilting (kinking), in the bilayer fluidity, and in the extent of disorder. In contrast, for the ID phase, the increase in a_{xy} (for c_M up to about 10 M) leads to no significant change in the bilayer thickness, to a slight increase in the degree of interpenetration of the two leaflets, and to a decrease in the extent of tilting, in the bilayer fluidity, and in the extent of disorder. These contrasting trends can be interpreted in terms of the mismatch between effective headgroup and tail cross-sections in the two phases. In the LC phase, the tail cross-section is too small for the headgroup one, and an increase in a_{xy} promotes an increase in disorder and fluidity. In the GL phase, the (doubled) tail cross-section is too large for the headgroup one (at least below $c_M \approx 10$ M), and an increase in a_{xy} now promotes an increase in order and rigidity.

The LC phase presents the highest extent of tilting (kinking) at the single lipid level, with a single-lipid tilt angle $\theta \approx 30\text{--}45^\circ$. However, these tilts (kinks) occur in random directions and the resulting collective tilt angle Θ is about 7.5° . The GL phase presents nearly equal single-lipid and collective tilt-angle values of about $\theta \approx 15\text{--}25^\circ$ and $\Theta \approx 10\text{--}25^\circ$. Here, the tilting of each leaflet is essentially collective, the simulations suggesting a preference for the relative tilt directions of the two leaflets at $\pm 60^\circ$ or $\pm 120^\circ$ from each other, with a precession time of about 50–100 ns in this angle. Because the leaflets consist here of a racemic mixture of the R and S enantiomers of GMP, positive and negative values in the relative tilt angle of the two leaflets should in principle be equally populated. The possible transmission of single-lipid chirality into a leaflet-twist chirality represents an interesting question, that could be investigated in the context of enantiomerically pure leaflets (RR, SS or RS). Work is in progress along these lines. The ID phase also presents nearly equal single-lipid and collective tilt-angle values of about $\theta \approx 8\text{--}20^\circ$ and $\Theta \approx 5\text{--}10^\circ$. These angles are much smaller than in the GL phase because optimal tail packing is reached via interdigitation, so that tilting (single-lipid as well as collective) is no longer necessary [60]. The simulations suggest a preference for relative tilt

directions of the two leaflets at 180° from each other, with a precession time of about 5–10 ns for the corresponding direction. A concerted (anti-parallel) precession for the two leaflets is expected here considering the interdigititation of the tails.

Finally, comparing the use of semi- and fully-anisotropic pressure scaling schemes in the simulations does not reveal striking differences in the phase properties and phase-transition temperatures. The release of the constraint on the proportions of the xy-plane (SEMI → FULL) slightly increases the estimated T_m for LC → ID transitions and decreases it for GL → LC transitions. However, these changes are probably not statistically significant.

Acknowledgements

Financial support from the Swiss National Foundation (Grants 21-132739 and 21-138020) is gratefully acknowledged.

Appendix A. Supplementary data

Supplementary data associated with this article can be found, in the online version, at <http://dx.doi.org/10.1016/j.jmgm.2014.10.017>.

References

- [1] G.M. Cooper, R.E. Hausman, *The Cell: A Molecular Approach*, ASM Press, Washington, DC, USA, 2007.
- [2] J.M. Seddon, G. Cevc, Lipid polymorphism: structure and stability of lyotropic mesophases of phospholipids, in: G. Cevc (Ed.), *Phospholipids Handbook*, Marcel Dekker, Inc., New York, USA, 1993, pp. 403–454.
- [3] I. Foubert, K. Dewettinck, D. van de Walle, A.J. Dijkstra, P.J. Quinn, Physical properties: structural and physical characteristics, in: F.D. Gunstone, J.L. Harwood, A.J. Dijkstra (Eds.), *The Lipid Handbook*, 3rd ed., CRC Press, Div. of Taylor, Francis Group, Boca Raton, USA, 2007, pp. 471–534.
- [4] J.F. Nagle, S. Tristram-Nagle, Structure of lipid bilayers, *Biochim. Biophys. Acta* 1469 (2000) 159.
- [5] G.R.A. Hunt, I.C. Jones, A¹H NMR investigation of the effects of ethanol and general anaesthetics on ion channels and membrane fusion using unilamellar phospholipid membranes, *Biochim. Biophys. Acta* 736 (1983) 1.
- [6] K.L. Pierce, R.T. Premont, R.J. Lefkowitz, Seven transmembrane receptors, *Nat. Rev. Mol. Cell Biol.* 3 (2002) 639.
- [7] L. Hicke, R. Dunn, Regulation of membrane protein transport by ubiquitin and ubiquitin-binding proteins, *Annu. Rev. Cell Dev. Biol.* 19 (2003) 141.
- [8] K. Kristiansen, Molecular mechanisms of ligand binding, signaling, and regulation within the superfamily of G-protein-coupled receptors: molecular modeling and mutagenesis approaches to receptor structure and function, *Pharmacol. Therap.* 103 (2004) 21.
- [9] J.H. Crowe, L.M. Crowe, J.F. Carpenter, C.A. Wistrom, Stabilization of dry phospholipid bilayers and proteins by sugar, *Biochem. J.* 242 (1987) 1.
- [10] B.W. Lee, R. Faller, A.K. Sum, I. Vattulainen, M. Patra, M. Karttunen, Structural effects of small molecules on phospholipid bilayers investigated by molecular simulations, *Fluid Phase Equil.* 225 (2004) 63.
- [11] J. Chanda, S. Bandyopadhyay, Perturbation of phospholipid bilayer properties by ethanol at a high concentration, *Langmuir* 22 (2006) 3775.
- [12] E. Yamamoto, T. Akimoto, H. Shimizu, Y. Hirano, M. Yasui, K. Yasuoka, Diffusive nature of xenon anesthetic changes properties of a lipid bilayer: molecular dynamics simulations, *J. Phys. Chem. B* 116 (2012) 8989.
- [13] G.L. Barchfeld, D.W. Deamer, Alcohol effects on lipid bilayer permeability to protons and potassium: relation to the action of general anaesthetics, *Biochim. Biophys. Acta* 944 (1988) 40.
- [14] R.S. Cantor, Breaking the Meyer–Overton rule: predicted effects of varying stiffness and interfacial activity on the intrinsic potency of anaesthetics, *Bioophys. J.* 80 (2001) 2284.
- [15] U. Rudolph, B. Antkowiak, Molecular and neuronal substrates for anaesthetics, *Nat. Rev. Neurosci.* 5 (2004) 709.
- [16] N.P. Franks, Molecular targets underlying general anaesthesia, *Br. J. Pharmacol.* 147 (2006) 72.
- [17] D. Keilin, The Leeuwenhoek lecture: the problem of anabiosis or latent life-history and current concept, *Proc. R. Soc. Lond. B Biol. Sci.* 150 (1959) 149.
- [18] J.C. Wright, Cryptobiosis 300 years on from van Leeuwenhoek: what have we learned about tardigrades, *Zool. Anz.* 240 (2001) 563.
- [19] J.S. Clegg, Cryptobiosis. A peculiar state of biological organization, *Comput. Biochem. Physiol. B* 128 (2001) 613.
- [20] E.P. Feovilova, Deceleration of vital activity as a universal biochemical mechanism ensuring adaptation of microorganisms to stress factors: a review, *Appl. Biochem. Microbiol.* 39 (2003) 1.
- [21] J.L. MacCallum, D.P. Tielemans, Interactions between small molecules and lipid bilayers, *Curr. Top. Membr.* 60 (2008) 227.
- [22] I. Ueda, H. Kamaya, Molecular mechanisms of anesthesia, *Anesth. Analg.* 63 (1984) 929.
- [23] N.P. Franks, General anaesthesia: from molecular targets to neuronal pathways of sleep and arousal, *Nat. Rev. Neurosci.* 9 (2008) 370.
- [24] Z. Fang, P. Ionescu, B.S. Chortkoff, L. Kandel, J. Sonner, M.J. Laster, E. Eger, Anesthetic potencies of n-alkanols: results of additivity and solubility studies suggest a mechanism of action similar to that for conventional inhaled anesthetics, *Anesth. Analg.* 84 (1997) 1042.
- [25] P.-L. Chau, New insights into the molecular mechanisms of general anaesthetics, *Br. J. Pharmacol.* 161 (2010) 288.
- [26] I. Ueda, T. Yoshida, Hydration of lipid membranes and the action mechanisms of anaesthetics and alcohols, *Chem. Phys. Lipids* 101 (1999) 65.
- [27] V. Castro, B. Stevenson, S.V. Dvinskikh, K.-J. Höglberg, A.P. Lyubartsev, H. Zimmermann, D. Sandström, A. Maliniak, NMR investigations of interactions between anaesthetics and lipid bilayers, *Biochim. Biophys. Acta* 1778 (2008) 2604.
- [28] R.S. Cantor, The lateral pressure profile in membranes: a physical mechanism of general anesthesia, *Biochemistry* 36 (1997) 2339.
- [29] E.S. Rowe, Lipid chain length and temperature dependence of ethanol–phosphatidylcholine interactions, *Biochemistry* 22 (1983) 3299.
- [30] E.S. Rowe, Thermodynamic reversibility of phase transitions. Specific effects of alcohols on phosphatidylcholines, *Biochim. Biophys. Acta* 813 (1985) 321.
- [31] S.A. Simon, T.J. McIntosh, Interdigitated hydrocarbon chain packing causes the biphasic transition behavior in lipid/alcohol suspensions, *Biochim. Biophys. Acta* 773 (1984) 169.
- [32] J.-S. Chiou, P.R. Krishna, H. Kamaya, I. Ueda, Alcohols dehydrate lipid membranes: an infrared study on hydrogen bonding, *Biochim. Biophys. Acta* 1110 (1992) 225.
- [33] J.A. Barry, K. Gawrisch, Direct NMR evidence for ethanol binding to the lipid–water interface of phospholipid bilayers, *Biochemistry* 33 (1994) 8082.
- [34] S.E. Feller, C.A. Brown, D.T. Nizza, K. Gawrisch, Nuclear Overhauser enhancement spectroscopy cross-relaxation rates and ethanol distribution across membranes, *Biophys. J.* 82 (2002) 1396.
- [35] J.M. Boggs, G. Rangaraj, Phase transitions and fatty acid spin label behavior in interdigitated lipid phases induced by glycerol and polymyxin, *Biochim. Biophys. Acta* 816 (1985) 221.
- [36] L. Löbecke, G. Cevc, Effects of short-chain alcohols on the phase behavior and interdigitation of phosphatidylcholine bilayer membrane, *Biochim. Biophys. Acta* 1237 (1995) 59.
- [37] L.L. Holte, K. Gawrisch, Determining ethanol distribution in phospholipid multilayers with MAS-NOESY spectra, *Biochemistry* 36 (1997) 4669.
- [38] H.V. Ly, D.E. Block, M.L. Longo, Interfacial tension effect of ethanol on lipid bilayer rigidity, stability and area/molecule: a micropipet aspiration approach, *Langmuir* 18 (2002) 8988.
- [39] H.V. Ly, M.L. Longo, The influence of short-chain alcohols on interfacial tension, mechanical properties, area/molecule, and permeability of fluid lipid bilayers, *Biophys. J.* 87 (2004) 1013.
- [40] K. Ohki, K. Tamura, I. Hatta, Ethanol induces interdigitated gel phase ($L_{\rho i}$) between lamellar gel phase (L_{β}) and ripple phase (P_{β}) in phosphatidylcholine membranes: a scanning density meter study, *Biochim. Biophys. Acta* 1023 (1990) 215.
- [41] J. Mou, J. Yang, C. Huang, Z. Shao, Alcohol induces interdigitated domains in unilamellar phosphatidylcholine bilayers, *Biochemistry* 33 (1994) 9981.
- [42] P.W. Westerman, J.M. Pope, N. Phonphok, J.W. Doane, D.W. Dubro, The interaction of n-alkanols with lipid bilayer membranes: a ²H NMR study, *Biochim. Biophys. Acta* 939 (1988) 64.
- [43] C.-H. Chen, K. Hoye, L.G. Roth, Thermodynamic and fluorescence studies of the underlying factors in benzyl alcohol-induced lipid interdigitated phase, *Arch. Biochem. Biophys.* 333 (1996) 401.
- [44] M. Kranenburg, M. Vlaar, B. Smit, Simulating induced interdigitation in membranes, *Biophys. J.* 87 (2004) 1596.
- [45] S.-J. Marrink, O. Berger, P. Tieleman, F. Jähnig, Adhesion forces of lipids in a phospholipid membrane studied by molecular dynamics simulations, *Biophys. J.* 74 (1998) 931.
- [46] E. Lindahl, O. Edholm, Spatial and energetic-entropic decomposition of surface tension in lipid bilayers from molecular dynamics simulations, *J. Chem. Phys.* 113 (2000) 3882.
- [47] C.S. Pereira, R.D. Lins, I. Chandrasekhar, L.C.G. Freitas, P.H. Hünenberger, Interaction of the disaccharide trehalose with a phospholipid bilayer: a molecular dynamics study, *Biophys. J.* 86 (2004) 2273.
- [48] B.W. Lee, R. Faller, A.K. Sum, I. Vattulainen, M. Patra, M. Karttunen, Structural effects of small molecules on phospholipid bilayers investigated by molecular simulations, *Fluid Phase Equil.* 228 (2005) 135.
- [49] A. Skibinsky, R.M. Venable, R.W. Pastor, A molecular dynamics study of the response of lipid bilayers and monolayers to trehalose, *Biophys. J.* 89 (2005) 4111.
- [50] A.M. Massari, I.J. Finkelstein, B.L. McClain, A. Goj, X. Wen, K.L. Bren, R.F. Loring, M.D. Fayer, The influence of aqueous versus glassy solvents on protein dynamics: vibrational echo experiments and molecular dynamics simulations, *J. Am. Chem. Soc.* 127 (2005) 14279.
- [51] M. Patra, E. Salonen, E. Terama, I. Vattulainen, R. Faller, B.W. Lee, J. Holopainen, M. Karttunen, Under the influence of alcohol: the effect of ethanol and methanol on lipid bilayers, *Biophys. J.* 90 (2006) 1121.
- [52] V. Knecht, S.-J. Marrink, Molecular dynamics simulations of lipid vesicle fusion in atomic detail, *Biophys. J.* 92 (2007) 4254.

- [53] C.S. Pereira, P.H. Hünenberger, The influence of polyhydroxylated compounds on a hydrated phospholipid bilayer: a molecular dynamics study, *Mol. Simul.* 34 (2008) 403.
- [54] B.A.C. Horta, A.H. de Vries, P.H. Hünenberger, Simulating the transition between gel and liquid-crystal phases of lipid bilayers: dependence of the transition temperature on the hydration level, *J. Chem. Theory Comput.* 6 (2010) 2488.
- [55] B.A.C. Horta, L. Perić-Hassler, P.H. Hünenberger, Interaction of the disaccharides trehalose and gentiobiose with lipid bilayers: a comparative molecular dynamics study, *J. Mol. Graph. Model.* 29 (2010) 331.
- [56] B.A.C. Horta, P.H. Hünenberger, Enantiomeric segregation in the gel phase of lipid bilayers, *J. Am. Chem. Soc.* 133 (2011) 8464.
- [57] M. Laner, B.A.C. Horta, P.H. Hünenberger, Phase-transition properties of glycerol-monopalmitate lipid bilayers investigated by molecular dynamics simulation: influence of the system size and force-field parameters, *Mol. Simul.* 39 (2013) 563.
- [58] A.P. Lyubartsev, A.L. Rabinovich, Recent development in computer simulation of lipid bilayers, *Soft Matter* 7 (2011) 25.
- [59] H. Saito, W. Shinoda, Cholesterol effect on water permeability through DPPC and PSM lipid bilayers: a molecular dynamics study, *J. Phys. Chem. B* 115 (2011) 15241.
- [60] M. Laner, B.A.C. Horta, P.H. Hünenberger, Long-timescale motions in glycerol-monopalmitate lipid bilayers investigated using molecular dynamics simulation, *J. Mol. Graph. Model.* 55 (2015) 48.
- [61] M. Laner, P.H. Hünenberger, Thermodynamics and kinetics of the gel to liquid-crystal phase transitions in glycerol-monopalmitate lipid bilayers: a Markovmodel analysis based on atomistic molecular dynamics simulations, *J. Chem. Theory Comput.* (submitted for publication).
- [62] M. Laner, P.H. Hünenberger, Phase-transition properties of glycerol-dipalmitate lipid bilayers investigated using molecular dynamics simulations, *Mol. Simul.* (submitted for publication).
- [63] A.N. Dickey, R. Faller, Investigating interactions of biomembranes and alcohols: a multiscale approach, *J. Polym. Sci. Part B: Polym. Phys.* 43 (2005) 1025.
- [64] A.A. Gurtovenko, J. Anwar, Interaction of ethanol with biological membranes: the formation of non-bilayer structures within the membrane interior and their significance, *J. Phys. Chem. B* 113 (2009) 1983.
- [65] C. Anézo, A.H. de Vries, H.-D. Höltje, D.P. Tieleman, S.-J. Marrink, Methodological issues in lipid bilayer simulations, *J. Phys. Chem. B* 107 (2003) 9424.
- [66] J.B. Klauda, R.M. Venable, A.D. MacKerell Jr., R.W. Pastor, Considerations for lipid force field development, *Curr. Top. Membr.* 60 (2008) 1.
- [67] S. McLaughlin, The electrostatic properties of membranes, *Annu. Rev. Biophys. Biophys. Chem.* 18 (1989) 113.
- [68] D.P. Tieleman, B. Hess, M.S.P. Sansom, Analysis and evaluation of channel models: simulation of alamethicin, *Biophys. J.* 83 (2002) 2393.
- [69] M. Patra, M. Karttunen, M.T. Hyvönen, E. Falck, P. Lindqvist, I. Vattulainen, Molecular dynamics simulations of lipid bilayers: major artifacts due to truncating electrostatic interactions, *Biophys. J.* 84 (2003) 3636.
- [70] M. Patra, M. Karttunen, M.T. Hyvönen, E. Falck, I. Vattulainen, Lipid bilayers driven to a wrong lane in molecular dynamics simulations by subtle changes in long-range electrostatic interactions, *J. Phys. Chem. B* 108 (2004) 4485.
- [71] M.A. Kastenholz, P.H. Hünenberger, Influence of artificial periodicity and ionic strength in molecular dynamics simulations of charged biomolecules employing lattice-sum methods, *J. Phys. Chem. B* 108 (2004) 774.
- [72] A. Cordomí, O. Edholm, J. Perez, Effect of different treatments of long-range interactions and sampling conditions in molecular dynamic simulations of rhodopsin embedded in a dipalmitoyl phosphatidylcholine bilayer, *J. Comput. Chem.* 28 (2007) 1017.
- [73] M.M. Reif, V. Kräutler, M.A. Kastenholz, X. Daura, P.H. Hünenberger, Explicit-solvent molecular dynamics simulations of a reversibly-folding β -heptapeptide in methanol: influence of the treatment of long-range electrostatic interactions, *J. Phys. Chem. B* 113 (2009) 3112.
- [74] Y. Takaoka, M. Pasenkiewicz-Gierula, H. Miyagawa, K. Kitamura, Y. Tamura, A. Kusumi, Molecular dynamics generation of nonarbitrary membrane models reveals lipid orientational correlations, *Biophys. J.* 79 (2000) 3118.
- [75] A.H. de Vries, I. Chandrasekhar, W.F. van Gunsteren, P.H. Hünenberger, Molecular dynamics simulations of phospholipid bilayers: influence of artificial periodicity, system size, and simulation time, *J. Phys. Chem.* 109 (2005) 11643.
- [76] D.H. Herce, A.E. Garcia, Correction of apparent finite size effects in the area per lipid of lipid membranes simulations, *J. Chem. Phys.* 125 (2006) 224711.
- [77] T. Bastug, S.M. Patra, S. Kuyucak, Finite system and periodicity effects in free energy simulations of membrane proteins, *Chem. Phys. Lett.* 425 (2006) 320.
- [78] J.B. Klauda, B.R. Brooks, R.W. Pastor, Dynamical motions of lipids and a finite size effect in simulations of bilayers, *J. Chem. Phys.* 125 (2006) 144710.
- [79] D.P. Tieleman, S.J. Marrink, H.J.C. Berendsen, A computer perspective of membranes: molecular dynamics studies of lipid bilayers systems, *Biochim. Biophys. Acta* 1331 (1997) 235.
- [80] S. Nagarajan, E.E. Schuler, K. Ma, J.T. Kindt, R.B. Dyer, Dynamics of the gel to fluid phase transformation in unilamellar DPPC vesicles, *J. Phys. Chem. B* 116 (2012) 13749.
- [81] M. Laner, B.A.C. Horta, P.H. Hünenberger, Effect of the cosolutes trehalose and methanol on the equilibrium and phase-transition properties of glycerol-monopalmitate lipid bilayers investigated using molecular dynamics simulations, *Eur. Biophys. J.* 43 (2014) 517.
- [82] W.R. Hargreaves, S.J. Mulvihill, Deamer, Synthesis of phospholipids and membranes in perbiotic conditions, *Nature* 3 (1976) 78.
- [83] F. Olasagasti, M.-C. Maurel, Deamer, Physico-chemical interactions between compartment-forming lipids and other prebiotically relevant biomolecules, *BIO Web Conf.* 2 (2014) 05001.
- [84] N. Krog, K. Larsson, Phase behaviour and rheological properties of aqueous systems of industrial distilled monoglycerides, *Chem. Phys. Lipids* 2 (1968) 129.
- [85] W.G. Morley, G.J.T. Tiddy, Phase behavior of monoglyceride/water systems, *J. Chem. Soc. Faraday Trans.* 89 (1993) 2823.
- [86] A.H. de Vries, S. Yefimov, A.E. Mark, S.J. Marrink, Molecular structure of the lecithin ripple phase, *Proc. Natl. Acad. Sci. U.S.A.* 102 (2005) 5392.
- [87] N. Krog, A.P. Borup, Swelling behaviour of lamellar phases of saturated monoglycerides in aqueous systems, *J. Sci. Fd. Agric.* 24 (1973) 691.
- [88] I. Pezon, E. Pezon, B.A. Bergenstahl, P.M. Claesson, Repulsive pressure between monoglyceride bilayers in the lamellar and gel states, *J. Phys. Chem.* 94 (1990) 8255.
- [89] I. Pezon, E. Pezon, P.M. Claesson, B.A. Bergenstahl, Monoglyceride surface films: stability and interlayer interactions, *J. Colloid Interface Sci.* 144 (1991) 449.
- [90] G. Cassin, C. de Costa, J.P.M. van Duynhoven, W.G.M. Agterof, Investigation of the gel to coagel phase transition in monoglyceride–water systems, *Langmuir* 14 (1998) 5757.
- [91] V. Chupin, J.-W.P. Boots, J.A. Killian, R.A. Demel, B. de Kruijff, Lipid organization and dynamics of the monostearoylglycerol–water system. A 2 H NMR study, *Chem. Phys. Lipids* 109 (2001) 15.
- [92] A. Sein, J.A. Verheij, W.G.M. Agterof, Rheological characterization, crystallization, and gelation behavior of monoglyceride gels, *J. Colloid Interface Sci.* 249 (2002) 412.
- [93] J.P.M. van Duynhoven, I. Broekmann, A. Sein, G.M.P. van Kempen, G.-J.W. Goudappel, W.S. Veeman, Microstructural investigation of monoglyceride–water coagel systems by NMR and CryoSEM, *J. Colloid Interface Sci.* 285 (2005) 703.
- [94] C. Alberola, B. Blümich, D. Emeis, K.-P. Wittern, Phase transitions of monoglyceride emulsifier systems and pearlescent effects in cosmetic creams studied by 13 C NMR spectroscopy and DSC, *Colloids Surf. A: Physicochem. Eng. Aspects 290 (2006) 247.*
- [95] N. Schmid, C.D. Christ, M. Christen, A.P. Eichenberger, W.F. van Gunsteren, Architecture implementation and parallelisation of the GROMOS software for biomolecular simulation, *Comput. Phys. Commun.* 183 (2012) 890.
- [96] A.-P.E. Kunz, J.R. Allison, D.P. Geerke, B.A.C. Horta, P.H. Hünenberger, S. Riniker, N. Schmid, W.F. van Gunsteren, New functionalities in the GROMOS biomolecular simulation software, *J. Comput. Chem.* 33 (2012) 340.
- [97] W.F. van Gunsteren, The GROMOS Software for Biomolecular Simulation. Available at: <http://www.gromos.net> 2011.
- [98] B.A.C. Horta, P.F.J. Fuchs, W.F. van Gunsteren, P.H. Hünenberger, New interaction parameters for oxygen compounds in the GROMOS force field: improved pure-liquid and solvation properties for alcohols, ethers, aldehydes, ketones, carboxylic acids and esters, *J. Chem. Theory Comput.* 7 (2011) 1016.
- [99] H.J.C. Berendsen, J.P.M. Postma, W.F. van Gunsteren, J. Hermans, Interaction models for water in relation to protein hydration, in: B. Pullman (Ed.), *Intermolecular Forces*, Reidel, Dordrecht, The Netherlands, 1981, pp. 331–342.
- [100] R.W. Hockney, The potential calculation and some applications, *Methods Comput. Phys.* 9 (1970) 136.
- [101] J.-P. Ryckaert, G. Ciccotti, H.J.C. Berendsen, Numerical integration of the Cartesian equations of motion of a system with constraints: molecular dynamics of *n*-alkanes, *J. Comput. Phys.* 23 (1977) 327.
- [102] S. Miyamoto, P.A. Kollman, SETTLE: an analytical version of the SHAKE and RATTLE algorithm for rigid water models, *J. Comput. Chem.* 13 (1992) 952.
- [103] H.J.C. Berendsen, J.P.M. Postma, W.F. van Gunsteren, A. di Nola, J.R. Haak, Molecular dynamics with coupling to an external bath, *J. Chem. Phys.* 81 (1984) 3684.
- [104] W.F. van Gunsteren, S.R. Billeter, A.A. Eising, P.H. Hünenberger, P. Krüger, A.E. Mark, W.R.P. Scott, I.G. Tironi, *Biomolecular Simulation: The GROMOS96 Manual and User Guide*, Verlag der Fachvereine, Zürich, Switzerland, 1996.
- [105] W.F. van Gunsteren, H.J.C. Berendsen, Computer simulation of molecular dynamics: methodology, applications and perspectives in chemistry, *Angew. Chem. Int. Ed.* 29 (1990) 992.
- [106] J.A. Barker, R.O. Watts, Monte Carlo studies of the dielectric properties of water-like models, *Mol. Phys.* 26 (1973) 789.
- [107] I.G. Tironi, R. Sperber, P.E. Smith, W.F. van Gunsteren, A generalized reaction field method for molecular dynamics simulations, *J. Chem. Phys.* 102 (1995) 5451.
- [108] T.N. Heinz, W.F. van Gunsteren, P.H. Hünenberger, Comparison of four methods to compute the dielectric permittivity of liquids from molecular dynamics simulations, *J. Chem. Phys.* 115 (2001) 1125.
- [109] S.Z. Mikhail, W.R. Kimel, Densities and viscosities of methanol–water mixtures, *J. Chem. Eng. Data* 6 (1961) 533.
- [110] E.S. Rowe, J.M. Campion, Alcohol induction of interdigitation in stearoylphosphatidylcholine: fluorescence studies of alcohol chain length requirements, *Biophys. J.* 67 (1994) 1888.
- [111] M.F.N. Rosser, H.M. Lu, P. Dea, Effect of alcohols on lipid bilayers with and without cholesterol: the dipalmitoylphosphatidylcholine system, *Biophys. Chem.* 81 (1999) 33.

- [112] D.M. Small, Lateral chain packing in lipids and membranes, *J. Lipid Res.* 25 (1984) 1490.
- [113] P. Westh, C. Trandum, Y. Koga, Binding of small alcohols to a lipid bilayer membrane: does the partition coefficient express the net affinity, *Biophys. Chem.* 89 (2001) 53.
- [114] C.S. Pereira, P.H. Hünenberger, Interaction of the sugars trehalose, maltose and glucose with a phospholipid bilayer: a comparative molecular dynamics study, *J. Phys. Chem. B* 110 (2006) 15572.
- [115] C.S. Pereira, P.H. Hünenberger, Effect of trehalose on a phospholipid membrane under mechanical stress, *Biophys. J.* 95 (2008) 3525.
- [116] J. Chanda, S. Chakraborty, S. Bandyopadhyay, Sensitivity of hydrogen bond lifetime dynamics to the presence of ethanol at the interface of a phospholipid bilayer, *J. Phys. Chem. B* 110 (2006) 3791.
- [117] Y. Okamoto, Generalized-ensemble algorithms: enhanced sampling techniques for Monte Carlo and molecular dynamics simulations, *J. Mol. Graph. Model.* 22 (2004) 425.
- [118] P. Minary, M. Levitt, Probing protein fold space with a simplified model, *J. Mol. Biol.* 375 (2008) 920.
- [119] M.S. Lee, M.A. Olson, Protein folding simulations combining self-guided Langevin dynamics and temperature-based replica exchange, *J. Chem. Theory Comput.* 6 (2010) 2477.
- [120] M.S. Lee, M.A. Olson, Comparison of two adaptive temperature-based replica exchange methods applied to a sharp phase transition of protein folding-unfolding, *J. Chem. Phys.* 134 (2011) 244111.
- [121] T. Nagai, Y. Okamoto, Replica-exchange molecular dynamics simulation of a lipid bilayer system with a coarse-grained model, *Mol. Simul.* 38 (2012) 437.